

Measurement of the Forward-Backward Asymmetry of $e^+e^- \rightarrow Z \rightarrow b\bar{b}$ using prompt leptons and a lifetime tag

DELPHI Collaboration

Abstract

The forward-backward asymmetry of the process $e^+e^- \rightarrow Z \rightarrow b\bar{b}$ has been measured using events collected by the DELPHI experiment during the 1991 and 1992 LEP runs. This data sample corresponded to 884 000 hadronic Z decays at a centre-of-mass energy $\sqrt{s} \sim M_Z$. The tagging of b-quark events was performed using two approaches; the first was based on the semileptonic decay channels $b \rightarrow X + \mu$ and $b \rightarrow X + e$, the second used a lifetime tag with jet-charge reconstruction. The results of these two methods were combined to give

$$A_{\text{FB}}^{b\bar{b}} = 0.107 \pm 0.011(\text{stat.} + \text{syst.} + \text{mixing}).$$

With the semileptonic sample, the forward-backward asymmetry of the process $e^+e^- \rightarrow Z \rightarrow c\bar{c}$ was also measured to be

$$A_{\text{FB}}^{c\bar{c}} = 0.083 \pm 0.022(\text{stat.}) \pm 0.016(\text{syst.}).$$

The effective value of the Weinberg mixing angle derived from these measurements was

$$\sin^2\theta_{\text{eff}}^{\text{lep}} = 0.2294 \pm 0.0021.$$

(To be submitted to Zeit. f. Physik C)

P.Abreu²⁰, W.Adam⁷, T.Adye³⁷, E.Agasi³⁰, I.Ajinenko⁴², R.Aleksan³⁹, G.D.Alekseev¹⁴, P.P.Allport²¹, S.Almehed²³, F.M.L.Almeida⁴⁷, S.J.Alvsvaag⁴, U.Amaldi⁷, A.Andreazza²⁷, P.Antilogos²⁴, W-D.Apel¹⁵, R.J.Apsimon³⁷, Y.Arnoud³⁹, B.Åsman⁴⁴, J-E.Augustin¹⁸, A.Augustinus³⁰, P.Baillon⁷, P.Bambade¹⁸, F.Barao²⁰, R.Barate¹², G.Barbiellini⁴⁶, D.Y.Bardin¹⁴, G.J.Barker³⁴, A.Baroncelli⁴⁰, O.Barring⁷, J.A.Barrio²⁵, W.Bartl⁵⁰, M.J.Bates³⁷, M.Battaglia¹³, M.Baubillier²², J.Baudot³⁹, K-H.Becks⁵², M.Begalli³⁶, P.Beilliere⁶, Yu.Belokopytov⁷, P.Beltran⁹, A.C.Benvenuti⁵, M.Berggren⁴¹, D.Bertrand², F.Bianchi⁴⁵, M.Big⁴⁵, M.S.Bilenky¹⁴, P.Billoir²², J.Bjarne²³, D.Bloch⁸, S.Blyth³⁴, V.Bocci³⁸, P.N.Bogolubov¹⁴, T.Bolognese³⁹, M.Bonesini²⁷, W.Bonivento²⁷, P.S.L.Booth²¹, G.Borisov⁴², C.Bosio⁴⁰, B.Bostjancic⁴³, S.Bosworth³⁴, O.Botner⁴⁸, B.Bouquet¹⁸, C.Bourdarios¹⁸, T.J.V.Bowcock²¹, M.Bozzo¹¹, S.Braibant², P.Branchini⁴⁰, K.D.Brand³⁵, R.A.Brenner¹³, H.Briand²², C.Bricman², L.Brillault²², R.C.A.Brown⁷, P.Bruckman¹⁶, J-M.Brunet⁶, L.Bugge³², T.Buran³², A.Buys⁷, M.Caccia²⁷, M.Calvi²⁷, A.J.Camacho Rozas⁴¹, R.Campion²¹, T.Camporesi⁷, V.Canale³⁸, K.Cankocak⁴⁴, F.Cao², F.Carena⁷, P.Carrillo⁴⁷, L.Carroll²¹, R.Cases⁴⁹, C.Caso¹¹, V.Cassio⁴⁵, M.V.Castillo Gimenez⁴⁹, A.Cattai⁷, F.R.Cavallo⁵, L.Cerrito³⁸, V.Chabaud⁷, A.Chan¹, Ph.Charpentier⁷, L.Chaussard²⁴, J.Chauveau²², P.Checchia³⁵, G.A.Chelkov¹⁴, P.Chliapnikov⁴², V.Chorowicz²², J.T.M.Chrin⁴⁹, V.Cindro⁴³, P.Collins³⁴, J.L.Contreras¹⁸, R.Contri¹¹, E.Cortina⁴⁹, G.Cosme¹⁸, F.Cossutti⁴⁶, F.Couchot¹⁸, H.B.Crawley¹, D.Crennell³⁷, G.Crosetti¹¹, J.Cuevas Maestro³³, S.Czellar¹³, E.Dahl-Jensen²⁸, J.Dahm⁵², B.Dalmagne¹⁸, M.Dam³², G.Damgaard²⁸, E.Daubie², A.Daum¹⁵, P.D.Dauncey³⁷, M.Davenport⁷, J.Davies²¹, W.Da Silva²², C.Defoix⁶, G.Della Ricca⁴⁶, P.Delpierre²⁶, N.Demaria³⁴, A.De Angelis⁷, H.De Boeck², W.De Boer¹⁵, S.De Brabandere², C.De Clercq², M.D.M.De Fez Laso⁴⁹, C.De La Vaissiere²², B.De Lotto⁴⁶, A.De Min²⁷, L.De Paula⁴⁷, C.De Saint-Jean³⁹, H.Dijkstra⁷, L.Di Ciaccio³⁸, F.Djama⁸, J.Dolbeau⁶, M.Donszelmann⁷, K.Doroba⁵¹, M.Dracos⁸, J.Drees⁵², M.Dris³¹, Y.Dufour⁶, F.Dupont¹², D.Edsall¹, R.Ehret¹⁵, T.Ekelof⁴⁸, G.Ekspong⁴⁴, M.Elsing⁵², J-P.Engel⁸, N.Ershaidat²², M.Espirito Santo²⁰, D.Fassouliotis³¹, M.Feindt⁷, A.Ferrer⁴⁹, T.A.Filippas³¹, A.Firestone¹, H.Foeth⁷, E.Fokitis³¹, F.Fontanelli¹¹, F.Formenti⁷, J-L.Fousset²⁶, B.Franek³⁷, P.Frenkel⁶, D.C.Fries¹⁵, A.G.Frodesen⁴, R.Fruhwrith⁵⁰, F.Fulda-Quenzer¹⁸, H.Furstenau⁷, J.Fuster⁷, D.Gamba⁴⁵, M.Gandelman¹⁷, C.Garcia⁴⁹, J.Garcia⁴¹, C.Gaspar⁷, U.Gasparini³⁵, Ph.Gavillet⁷, E.N.Gazis³¹, D.Gele⁸, J-P.Gerber⁸, L.Gerdyukov⁴², D.Gillespie⁷, R.Gokieli⁵¹, B.Golob⁴³, V.M.Golovatyuk¹⁴, J.J.Gomez Y Cadenas⁷, G.Gopal³⁷, L.Gorn¹, M.Gorski⁵¹, V.Gracco¹¹, F.Grad², E.Graziani⁴⁰, G.Grosdidier¹⁸, P.Gunnarsson⁴⁴, J.Guy³⁷, U.Haeding¹⁵, F.Hahn⁵², M.Hahn⁴⁴, S.Hahn⁵², S.Haider³⁰, Z.Hajduk¹⁶, A.Hakansson²³, A.Hallgren⁴⁸, K.Hamacher⁵², W.Hao³⁰, F.J.Harris³⁴, V.Hedberg²³, R.Henriques²⁰, J.J.Hernandez⁴⁹, J.A.Hernando⁴⁹, P.Herquet², H.Herr⁷, T.L.Hessing⁷, E.Higon⁴⁹, H.J.Hilke⁷, T.S.Hill¹, S-O.Holmgren⁴⁴, P.J.Holt³⁴, D.Holthuizen³⁰, P.F.Honore⁶, M.Houlden²¹, J.Hrubec⁵⁰, K.Huet², K.Hultqvist⁴⁴, P.Ioannou³, P-S.Iversen⁴, J.N.Jackson²¹, R.Jacobsson⁴⁴, P.Jalocha¹⁶, G.Jarlskog²³, P.Jarry³⁹, B.Jean-Marie⁴⁴, E.K.Johansson⁴⁴, L.Jonsson²³, P.Juillot⁸, M.Kaiser¹⁵, G.Kalmus³⁷, F.Kapusta²², M.Karlsson⁴⁴, E.Karvelas⁹, S.Katsanevas³, E.C.Katsoufis³¹, R.Keranen⁷, B.A.Khomenko¹⁴, N.N.Khovanski¹⁴, B.King²¹, N.J.Kjaer²⁸, H.Klein⁷, A.Klovning⁴, P.Kluit³⁰, A.Koch-Mehrin⁵², J.H.Koehne¹⁵, B.Koene³⁰, P.Kokkinias⁹, M.Koratzinos⁷, A.V.Korytov¹⁴, V.Kostioukhine⁴², C.Kourkoumelis³, O.Kouznetsov¹¹, P-H.Kramer⁵², M.Krammer⁵⁰, C.Kreuter¹⁵, J.Krolkowski⁵¹, I.Kronkvist²³, W.Krupinski¹⁶, W.Kucewicz¹⁶, K.Kulka⁴⁸, K.Kurvinen¹³, C.Lacasta⁴⁹, I.Laktineh²⁴, C.Lambropoulos⁹, J.W.Lamsa¹, L.Lanceri⁴⁶, P.Langefeld⁵², V.Lapin⁴², I.Last²¹, J-P.Laugier³⁹, R.Lauhakangas¹³, G.Leder⁵⁰, F.Ledroit¹², R.Leitner²⁹, Y.Lemoigne³⁹, J.Lemonne², G.Lenzen⁵², V.Lepeltier¹⁸, J.M.Levy⁸, E.Lieb⁵², D.Liko⁵⁰, R.Lindner⁵², A.Lipniacka¹⁸, I.Lippi³⁵, B.Loerstad²³, M.Lokajicek¹⁰, J.G.Loken³⁴, A.Lopez-Fernandez⁷, M.A.Lopez Aguerá⁴¹, M.Los³⁰, D.Loukas⁹, J.J.Lozano⁴⁹, P.Lutz³⁹, L.Lyons³⁴, G.Maehlum¹⁵, J.Maillard⁶, A.Maio²⁰, A.Maltezos⁹, F.Mandl⁵⁰, J.Marco⁴¹, B.Marechal⁴⁷, M.Margoni³⁵, J-C.Marin⁷, C.Mariotti⁴⁰, A.Markou⁹, T.Marou⁵², S.Marti⁴⁹, C.Martinez-Rivero⁴¹, F.Martinez-Vidal⁴⁹, F.Matorras⁴¹, C.Matteuzzi²⁷, G.Matthiae³⁸, M.Mazzucato³⁵, M.Mc Cubbin⁷, R.Mc Kay¹, R.Mc Nulty²¹, J.Medbo⁴⁸, C.Meroni²⁷, W.T.Meyer¹, A.Miagkov⁴², M.Michelotto³⁵, E.Migliore⁴⁵, L.Mirabito²⁴, W.A.Mitaroff⁵⁰, G.V.Mitselmakher¹⁴, U.Mjoernmark²³, T.Moa⁴⁴, R.Moeller²⁸, K.Moenig⁷, M.R.Monge¹¹, P.Morettini¹¹, H.Mueller¹⁵, W.J.Murray³⁷, B.Muryn¹⁶, G.Myatt³⁴, F.Naraghi¹², F.L.Navarria⁵, P.Negri²⁷, S.Nemecek¹⁰, W.Neumann⁵², N.Neumeister⁵⁰, R.Nicolaidou³, B.S.Nielsen²⁸, V.Nikolaenko²⁴, P.Niss⁴⁴, A.Nomerotski³⁵, A.Normand³⁴, V.Obraztsov⁴², A.G.Olshevski¹⁴, R.Orava¹³, K.Osterberg¹³, A.Ouraou³⁹, P.Paganini¹⁸, M.Paganoni²⁷, R.Pain²², H.Palka¹⁶, Th.D.Papadopoulou³¹, L.Pape⁷, F.Parodi¹¹, A.Passerio⁴⁰, M.Pegoraro³⁵, J.Pennanen¹³, L.Peralta²⁰, H.Pernegger⁵⁰, M.Pernicka⁵⁰, A.Perrotta⁵, C.Petridou⁴⁶, A.Petrolini¹¹, H.T.Phillips³⁷, G.Piana¹¹, F.Pierre³⁹, M.Pimenta²⁰, S.Plaszczynski¹⁸, O.Podobrin¹⁵, M.E.Pol¹⁷, G.Polk¹⁶, P.Poropat⁴⁶, V.Pozdniakov¹⁴, M.Prest⁴⁶, P.Privitera³⁸, A.Pullia²⁷, D.Radojicic³⁴, S.Ragazzi²⁷, H.Rahmani³¹, J.Rames¹⁰, P.N.Ratoff¹⁹, A.L.Read³², M.Reale⁵², P.Rebecchi¹⁸, N.G.Redaeli²⁷, M.Regler⁵⁰, D.Reid⁷, P.B.Renton³⁴, L.K.Resvanis³⁴, F.Richard¹⁸, J.Richardson²¹, J.Ridky¹⁰, G.Rinaudo⁴⁵, I.Ripp³⁹, A.Romero⁴⁵, I.Roncagliolo¹¹, P.Ronchese³⁵, L.Roos¹², E.I.Rosenberg¹, E.Rosso⁷, P.Roudeau¹⁸, T.Rovelli⁵, W.Ruckstuhl³⁰, V.Ruhlmann-Kleider³⁹, A.Ruiz⁴¹, H.Saarikko¹³, Y.Sacquin³⁹, G.Sajot¹², J.Salt⁴⁹, J.Sanchez²⁵, M.Sannino¹¹, H.Schneider¹⁵, M.A.E.Schyns⁵², G.Sciolla⁴⁵, F.Scuri⁴⁶, A.M.Segar³⁴, A.Seitz¹⁵, R.Sekulin³⁷, R.Seufert¹⁵, R.C.Shellard³⁶, I.Siccamo³⁰, P.Siegrist³⁹, S.Simonetti³⁹, F.Simonetto³⁵, A.N.Sisakian¹⁴, T.B.Skaali³², G.Smadya²⁴, N.Smirmov⁴², O.Smirmova¹⁴, G.R.Smith³⁷, A.Sokolov⁴², R.Sosnowski⁵¹, D.Souza-Santos³⁶, T.Spassov²⁰, E.Spiriti⁴⁰, S.Squarcia¹¹, H.Staek⁵², C.Stanescu⁴⁰, S.Stapnes³², I.Stavitski³⁵, G.Stavropoulos⁹, K.Stepaniak⁵¹, F.Stichelbaut⁷, A.Stocchi¹⁸, J.Strauss⁵⁰, J.Straver⁷, R.Strub⁸, B.Stugu⁴, M.Szczekowski⁵¹, M.Szeptycka⁵¹,

T.Tabarelli²⁷, O.Tchikilev⁴², G.E.Theodosiou⁹, Z.Thome⁴⁷, A.Tilquin²⁶, J.Timmermans³⁰, V.G.Timofeev¹⁴, L.G.Tkatchev¹⁴, T.Todorov⁸, D.Z.Toet³⁰, A.Tomaradze², B.Tome²⁰, E.Torassa⁴⁵, L.Tortora⁴⁰, G.Transtromer²³, D.Treille⁷, W.Trischuk⁷, G.Tristram⁶, C.Troncon²⁷, A.Tsirou⁷, E.N.Tsyganov¹⁴, M-L.Turluer³⁹, T.Tuuva¹³, I.A.Tyapkin²², M.Tyndel³⁷, S.Tzamarías²¹, B.Ueberschaer⁵², S.Ueberschaer⁵², O.Ullaland⁷, V.Uvarov⁴², G.Valenti⁵, E.Vallazza⁷, J.A.Valls Ferrer⁴⁹, C.Vander Velde², G.W.Van Apeldoorn³⁰, P.Van Dam³⁰, M.Van Der Heijden³⁰, W.K.Van Doninck², J.Van Eldik³⁰, G.Vegni²⁷, L.Ventura³⁵, W.Venus³⁷, F.Verbeure², M.Verlato³⁵, L.S.Vertogradov¹⁴, D.Vilanova³⁹, P.Vincent²⁴, L.Vitale⁴⁶, E.Vlasov⁴², A.S.Vodopyanov¹⁴, M.Vollmer⁵², M.Voutilainen¹³, V.Vrba¹⁰, H.Wahlen⁵², C.Walck⁴⁴, A.Wehr⁵², M.Weierstall⁵², P.Weilhammer⁷, A.M.Wetherell⁷, J.H.Wickens², M.Wielers¹⁵, G.R.Wilkinson³⁴, W.S.C.Williams³⁴, M.Winter⁸, M.Witek⁷, G.Wormser¹⁸, K.Woschnagg⁴⁸, K.Yip³⁴, O.Yushchenko⁴², F.Zach²⁴, A.Zaitsev⁴², A.Zalewska¹⁶, P.Zalewski⁵¹, D.Zavrtanik⁴³, E.Zevgolatakos⁹, N.I.Zimin¹⁴, M.Zito³⁹, D.Zontar⁴³, R.Zuberi³⁴, G.Zumerle³⁵

¹ Ames Laboratory and Department of Physics, Iowa State University, Ames IA 50011, USA

² Physics Department, Univ. Instelling Antwerpen, Universiteitsplein 1, B-2610 Wilrijk, Belgium and IIHE, ULB-VUB, Pleinlaan 2, B-1050 Brussels, Belgium and Faculté des Sciences, Univ. de l'Etat Mons, Av. Maistriau 19, B-7000 Mons, Belgium

³ Physics Laboratory, University of Athens, Solonos Str. 104, GR-10680 Athens, Greece

⁴ Department of Physics, University of Bergen, Allégaten 55, N-5007 Bergen, Norway

⁵ Dipartimento di Fisica, Università di Bologna and INFN, Via Irnerio 46, I-40126 Bologna, Italy

⁶ Collège de France, Lab. de Physique Corpusculaire, IN2P3-CNRS, F-75231 Paris Cedex 05, France

⁷ CERN, CH-1211 Geneva 23, Switzerland

⁸ Centre de Recherche Nucléaire, IN2P3 - CNRS/ULP - BP20, F-67037 Strasbourg Cedex, France

⁹ Institute of Nuclear Physics, N.C.S.R. Demokritos, P.O. Box 60228, GR-15310 Athens, Greece

¹⁰ FZU, Inst. of Physics of the C.A.S. High Energy Physics Division, Na Slovance 2, 180 40, Praha 8, Czech Republic

¹¹ Dipartimento di Fisica, Università di Genova and INFN, Via Dodecaneso 33, I-16146 Genova, Italy

¹² Institut des Sciences Nucléaires, IN2P3-CNRS, Université de Grenoble 1, F-38026 Grenoble Cedex, France

¹³ Research Institute for High Energy Physics, SEFT, P.O. Box 9, FIN-00014 Helsinki, Finland

¹⁴ Joint Institute for Nuclear Research, Dubna, Head Post Office, P.O. Box 79, 101 000 Moscow, Russian Federation

¹⁵ Institut für Experimentelle Kernphysik, Universität Karlsruhe, Postfach 6980, D-76128 Karlsruhe, Germany

¹⁶ High Energy Physics Laboratory, Institute of Nuclear Physics, Ul. Kawiorów 26a, PL-30055 Krakow 30, Poland

¹⁷ Centro Brasileiro de Pesquisas Físicas, rua Xavier Sigaud 150, BR-22290 Rio de Janeiro, Brazil

¹⁸ Université de Paris-Sud, Lab. de l'Accélérateur Linéaire, IN2P3-CNRS, Bat 200, F-91405 Orsay Cedex, France

¹⁹ School of Physics and Materials, University of Lancaster, Lancaster LA1 4YB, UK

²⁰ LIP, IST, FCUL - Av. Elias Garcia, 14-1º, P-1000 Lisboa Codex, Portugal

²¹ Department of Physics, University of Liverpool, P.O. Box 147, Liverpool L69 3BX, UK

²² LPNHE, IN2P3-CNRS, Universités Paris VI et VII, Tour 33 (RdC), 4 place Jussieu, F-75252 Paris Cedex 05, France

²³ Department of Physics, University of Lund, Sölvegatan 14, S-22363 Lund, Sweden

²⁴ Université Claude Bernard de Lyon, IPNL, IN2P3-CNRS, F-69622 Villeurbanne Cedex, France

²⁵ Universidad Complutense, Avda. Complutense s/n, E-28040 Madrid, Spain

²⁶ Univ. d'Aix - Marseille II - CPP, IN2P3-CNRS, F-13288 Marseille Cedex 09, France

²⁷ Dipartimento di Fisica, Università di Milano and INFN, Via Celoria 16, I-20133 Milan, Italy

²⁸ Niels Bohr Institute, Blegdamsvej 17, DK-2100 Copenhagen 0, Denmark

²⁹ NC, Nuclear Centre of MFF, Charles University, Areal MFF, V Holesovickach 2, 180 00, Praha 8, Czech Republic

³⁰ NIKHEF-H, Postbus 41882, NL-1009 DB Amsterdam, The Netherlands

³¹ National Technical University, Physics Department, Zografou Campus, GR-15773 Athens, Greece

³² Physics Department, University of Oslo, Blindern, N-1000 Oslo 3, Norway

³³ Dpto. Fisica, Univ. Oviedo, C/P. Pérez Casas, S/N-33006 Oviedo, Spain

³⁴ Department of Physics, University of Oxford, Keble Road, Oxford OX1 3RH, UK

³⁵ Dipartimento di Fisica, Università di Padova and INFN, Via Marzolo 8, I-35131 Padua, Italy

³⁶ Depto. de Fisica, Pontificia Univ. Católica, C.P. 38071 RJ-22453 Rio de Janeiro, Brazil

³⁷ Rutherford Appleton Laboratory, Chilton, Didcot OX11 0QX, UK

³⁸ Dipartimento di Fisica, Università di Roma II and INFN, Tor Vergata, I-00173 Rome, Italy

³⁹ Centre d'Etude de Saclay, DSM/DAPNIA, F-91191 Gif-sur-Yvette Cedex, France

⁴⁰ Istituto Superiore di Sanità, Ist. Naz. di Fisica Nucl. (INFN), Viale Regina Elena 299, I-00161 Rome, Italy

⁴¹ C.E.A.F.M., C.S.I.C. - Univ. Cantabria, Avda. los Castros, S/N-39006 Santander, Spain, (CICYT-AEN93-0832)

⁴² Inst. for High Energy Physics, Serpukov P.O. Box 35, Protvino, (Moscow Region), Russian Federation

⁴³ J. Stefan Institute and Department of Physics, University of Ljubljana, Jamova 39, SI-61000 Ljubljana, Slovenia

⁴⁴ Fysikum, Stockholm University, Box 6730, S-113 85 Stockholm, Sweden

⁴⁵ Dipartimento di Fisica Sperimentale, Università di Torino and INFN, Via P. Giuria 1, I-10125 Turin, Italy

⁴⁶ Dipartimento di Fisica, Università di Trieste and INFN, Via A. Valerio 2, I-34127 Trieste, Italy and Istituto di Fisica, Università di Udine, I-33100 Udine, Italy

⁴⁷ Univ. Federal do Rio de Janeiro, C.P. 68528 Cidade Univ., Ilha do Fundão BR-21945-970 Rio de Janeiro, Brazil

⁴⁸ Department of Radiation Sciences, University of Uppsala, P.O. Box 535, S-751 21 Uppsala, Sweden

⁴⁹ IFIC, Valencia-CSIC, and D.F.A.M.N., U. de Valencia, Avda. Dr. Moliner 50, E-46100 Burjassot (Valencia), Spain

⁵⁰ Institut für Hochenergiephysik, Österr. Akad. d. Wissensch., Nikolsdorfergasse 18, A-1050 Vienna, Austria

⁵¹ Inst. Nuclear Studies and University of Warsaw, Ul. Hoza 69, PL-00681 Warsaw, Poland

⁵² Fachbereich Physik, University of Wuppertal, Postfach 100 127, D-42097 Wuppertal 1, Germany

1 Introduction

For the reaction $e^+e^- \rightarrow Z \rightarrow b\bar{b}$, the distribution of the b -quark angle θ_b relative to the e^- direction can be expressed as:

$$\frac{d\sigma}{d\cos\theta_b} \propto 1 + \cos^2\theta_b + \frac{8}{3}A_{\text{FB}}^{b\bar{b}} \cos\theta_b. \quad (1)$$

In the context of the Standard Model the parity violating asymmetry term $A_{\text{FB}}^{b\bar{b}}$ is related to the vector (v_f) and axial (a_f) couplings of the fermions to the Z boson. To lowest order $A_{\text{FB}}^{b\bar{b}}$ at $\sqrt{s} = M_Z$ is given by

$$A_{\text{FB}}^{b\bar{b}} \approx \frac{3}{4} \frac{2a_e v_e}{a_e^2 + v_e^2} \frac{2a_b v_b}{a_b^2 + v_b^2}.$$

Higher-order radiative corrections modify the tree-level relations. The electro-weak corrections can be accounted for using an analogous relation for $A_{\text{FB}}^{b\bar{b}}$, but with modified couplings \bar{v}_f, \bar{a}_f for the fermions, and an effective value θ_{eff}^f of the Weinberg angle defined by

$$\frac{\bar{v}_f}{\bar{a}_f} = 1 - 4|q_f| \sin^2\theta_{eff}^f$$

where q_f is the electric charge of the fermion. All the effects due to the top-quark and Higgs-boson masses are contained in this effective quantity. The forward-backward asymmetry in $Z \rightarrow b\bar{b}$ events has a high sensitivity to $\sin^2\theta_{eff}^f$. Therefore the precise knowledge of $A_{\text{FB}}^{b\bar{b}}$ allows an accurate test of the Standard Model.

In this paper, a measurement of $A_{\text{FB}}^{b\bar{b}}$ at LEP with the DELPHI detector using events collected in 1991 and 1992 is presented. Two independent techniques were followed to perform this measurement. The first used the semileptonic decays of the b -quark into muons and electrons, exploiting the charge correlation between the parent b -quark and the decay lepton. Similar analyses have been previously published, by DELPHI using muonic events collected in 1990 [1], and by other LEP experiments [2–4]. The second approach exploits a decay tag using a high-resolution vertex detector to select an enriched B-sample, and was used in [5]. The original b -quark charge was obtained using a hemisphere jet-charge algorithm. In both approaches, the thrust axis of the event [6] was used to approximate the original b -quark direction.

2 Event selection

2.1 The DELPHI detector

The reference frame used in the present analysis has the z-axis along the beam direction and oriented with the incoming e^- . The polar angle θ is defined with respect to the z-axis, and the azimuthal angle ϕ in the $R\phi$ plane perpendicular to the beam.

The DELPHI detector has been described in detail elsewhere [7]. Only those components which were used in this analysis are discussed here. The tracking of charged particles was accomplished with a set of cylindrical tracking detectors whose axes were oriented along the 1.23 T magnetic field and the direction of the beam. The Vertex Detector (VD), located nearest to the LEP interaction region, consisted of three concentric layers of silicon microstrip detectors at average radii of 6.3 cm, 8.8 cm, and 10.9 cm covering the central region of the DELPHI apparatus at polar angles θ between 27° and

153°. A beryllium beam pipe with a radius of 5.5 cm was installed in 1991, which allowed the innermost layer of silicon microstrip detectors to be added at a radius of 6.3 cm. Outside the VD between radii of 12 cm and 28 cm was the Inner Detector (ID), which was composed of a jet chamber giving up to 24 measurements in the $R\phi$ plane. The VD and ID were surrounded by the main DELPHI tracking device, the Time Projection Chamber (TPC), which provided up to 16 space points between radii of 30 cm and 122 cm. The Outer Detector (OD) at a radius of 198 cm to 206 cm consisted of five layers of drift cells. In the forward regions two sets of tracking chambers, at ± 160 cm and ± 270 cm in z , completed the charged-particle reconstruction at low angle. The average momentum resolution of the tracking system was measured to be $\sigma_p/p = 0.001 p$ (p in GeV/c), in the polar region between 30° and 150°. After the alignment corrections had been applied, the resolution of the extrapolation to the event vertex was measured using high-momentum muons from $Z \rightarrow \mu^+ \mu^-$ events. The value of $(26 \pm 2) \mu\text{m}$ [8] for the asymptotic charged-particle track extrapolation error was obtained.

The muon identification relied mainly on the muon chambers, a set of drift chambers with three-dimensional information situated at the periphery of DELPHI after approximately 1 m of iron. One set of chambers was located 20 cm before the end of the hadronic calorimeter, two further sets of chambers being outside. In the Barrel part of the detector ($|\cos \theta| < 0.63$) there were three layers each including two active planes of chambers. The two external layers overlap in azimuth to avoid dead spaces. In the Forward part, the inner and outer layers consisted of two planes of drift chambers with anode wires crossed at right angles. The resolution was 1.0 cm in z and 0.2 cm in $R\phi$ for the Barrel part and 0.4 cm for the Forward one. Near 90° to the beam, there were 7.5 absorption lengths between the interaction point and the last muon detector.

The electromagnetic calorimeter in the barrel region ($|\cos \theta| < 0.73$) was the High density Projection Chamber (HPC), situated inside the superconducting coil. The detector had a thickness of 17.5 radiation lengths and consisted of 144 modules arranged in 6 rings along z , each module was divided into 9 drift layers separated by lead. It provided three-dimensional shower reconstruction. In the forward region ($0.80 < |\cos \theta| < 0.98$) the electromagnetic calorimeter FEMC consisted of two 5-meter diameter disks with a total of 9064 lead-glass blocks in the form of truncated pyramids, arranged almost to point towards the interaction region.

2.2 The sample of hadronic events

For the reconstruction of the hadronic events, the following selection was applied: Charged-particle tracks were required to have:

1. a polar angle such that $|\cos \theta| < 0.93$;
2. a track length between the first and last measured point larger than 30 cm;
3. an impact parameter in $R\phi$ less than 5 cm and in $|z|$ less than 10 cm;
4. a momentum p greater than 0.2 GeV/c with a relative error $\frac{\sigma_p}{p}$ less than 1.

Neutral clusters were required to:

1. be detected by the HPC or the FEMC;
2. have polar angle such that $|\cos \theta| < 0.98$;
3. have an energy greater than 0.8 (0.4) GeV in the barrel (end-caps).

Hadronic events were selected which contained:

1. at least 7 accepted charged particles;

2. a total measured energy of these charged particles (assuming pion masses) larger than $0.15 \sqrt{s}$;

The $\tau^+\tau^-$ and photon-photon final states remaining after the energy and multiplicity cuts represented a negligible fraction of the selected sample (below 0.1%).

Only the data collected near the Z peak (91.27 ± 0.2) GeV were used in the present analysis corresponding to a sample of 689 000 (195 000) hadronic events respectively for the 1992 (1991) data.

The JETSET 7.3 model [9] was used to generate Monte Carlo events. The Lund symmetric fragmentation function [9] described the hadronisation of the u , d , s quarks while the fragmentation of heavy quarks, c and b , was parameterised by a Peterson function [10]. In this analysis, the simulated events were reweighted to match the most recently measured values. The corresponding fragmentation parameters and the semi-leptonic branching ratios used are given in section 3.2. The response of the DELPHI detector to the generated events was simulated using the program DELSIM [11]. For most of the studies presented below, samples of 466 000 simulated events for 1992 and 171 000 events for 1991 were used.

3 $A_{\text{FB}}^{\text{b}\bar{\text{b}}}$ measurement using leptons

The main kinematical variable used to measure the flavour composition of the leptonic events was the transverse momentum of the lepton with respect to the closest jet. The value of this variable depends on the jet reconstruction algorithm. Jets were reconstructed using the JADE algorithm [12] with a scaled invariant mass cut $y_{\text{cut}} = \frac{m_j^2}{E_{\text{vis}}^2} \geq 0.01$. Charged and neutral particles were used for the jet reconstruction. The transverse momentum, p_t , of the lepton is defined as the momentum transverse to the jet axis when the lepton is excluded from the jet definition. Leptons having an angle greater than 90° with this jet axis were rejected. When the lepton was the only particle in the jet, it was associated to the closest jet in the same hemisphere, defined by the plane perpendicular to the thrust axis at the production point. If the lepton was the only particle of the hemisphere, its p_t was set to 0. This algorithm was chosen so as to optimise the sample purity and showed good agreement between data and predictions from simulation.

To ensure a good determination of the jet and thrust polar angle θ_T , the analysis was limited to events with $|\cos \theta_T| < 0.9$ for the μ sample. As electrons were only identified in the barrel region, a cut $|\cos \theta_T| < 0.7$ was applied in that case to avoid artificially enriching the sample with events with high sphericity. Events with more than one lepton candidate were used once per candidate. This approach reduces the efficiency dependence of the result. It has been checked that there is a negligible difference between the statistical precision obtained by this method and by the one using only one lepton candidate per event.

3.1 Lepton identification

3.1.1 Muon sample

Muon candidates were identified using the muon chambers. The tracks found in the central detectors define a road along which hits in the muon chambers were searched for. The identification algorithm was described extensively in [13]. Muon candidates with momentum above 3 GeV/ c and in the region of good geometrical acceptance were

selected. It was required that $0.03 < |\cos \theta_\mu| < 0.6$ or $0.68 < |\cos \theta_\mu| < 0.93$ where θ_μ was the muon polar angle. The efficiency of the muon identification for this sample was estimated to be $(86.4 \pm 0.3)\%$ in the simulation.

The identification efficiency for muons was checked in $Z \rightarrow \mu^+\mu^-$, $Z \rightarrow \tau^+\tau^-$ and $\gamma\gamma \rightarrow \mu^+\mu^-$ events. The ratio of the efficiencies in the data and in the simulation was $(97.9 \pm 0.5)\%$ above 35 GeV/c and $(96.2 \pm 2.5)\%$ below 35 GeV/c with a small θ dependence. Corrections were made for these efficiency discrepancies between data and simulation. To determine from the data the efficiency of the identification algorithm in hadronic events, the number of reconstructed J/ψ events was measured, requesting that one or two muons be identified. An efficiency of $(86.8 \pm 4.0)\%$ was found while the simulation predicted a value of $(86.2 \pm 4.9)\%$. From these studies, the relative uncertainty on the efficiency was estimated to be $\pm 3\%$.

Since the difference between the number of positive and negative particles was computed in small θ intervals, the sensitivity to the efficiency was small, but to extract the experimental b -quark asymmetry $A_{\text{FB}}^{b,\text{exp}}$ from the observed asymmetry, the correct description of the fraction of background in the sample was needed. The contamination from misidentified hadrons arose partly from the decay of pions and kaons, but mostly from high-energy hadrons which interacted deep in the calorimeter and generated ‘punch-through’. The decays of τ particles into three pions were used to check that the rate of pion misidentification was properly estimated by the simulation program. For example, in the 1992 data sample, the fraction of misidentified pions obtained was $(0.92 \pm 0.16)\%$ while it was $(0.83 \pm 0.08)\%$ in the simulation. The same conclusion was obtained with a pion sample coming from K_S^0 decays.

To monitor the description of the background, the number of muon candidates normalized to the number of hadronic Z decays was compared between data and simulation in different kinematical regions. The high- p , high- p_t region was used to define an overall efficiency, while the low- p , low- p_t region, highly sensitive to the background level, allowed a fine control of the background description. The results found were compatible with the previously mentioned efficiency difference between data and simulation. The shape of the data distributions were seen to be compatible with the background level predicted by the simulation. A systematic error of $\pm 15\%$ has been attributed to the estimated hadronic background.

Most of the high momentum particles generating the ‘punch-through’ were correlated in sign with the initial quark of the event. The tracks involved in this charge correlation are mostly kaons coming from $e^+e^- \rightarrow Z \rightarrow b\bar{b}$ ($b \rightarrow c \rightarrow s$), $e^+e^- \rightarrow Z \rightarrow c\bar{c}$ ($c \rightarrow s$) or $e^+e^- \rightarrow Z \rightarrow s\bar{s}$ events. The simulation was used to estimate the contribution of the fake muons to the observed asymmetry as described in section 3.3.

Another important point for this analysis is that the correct charge be assigned to the particles. For charged particles in the kinematical region of the leptonic sample no error in the charge attribution was observed in DELPHI.

Taking into account all selections applied to the muon sample (hadronic selection, track selection, angular and momentum selection), a total identification efficiency of $(46 \pm 1)\%$ was estimated for muons coming from direct b semi-leptonic decay. The comparison between the data and the shape predicted by the simulation for the p and p_t spectra is presented for the muon sample on figures 1 and 2, and on figures 3 and 4 for the electron sample (see following subsection). The corresponding $\cos \theta_T$ distributions are shown on figures 5 and 6.

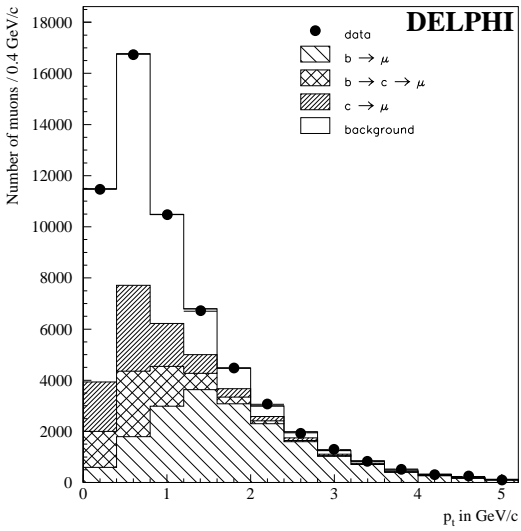


Figure 1: Transverse-momentum distribution of muon candidates.

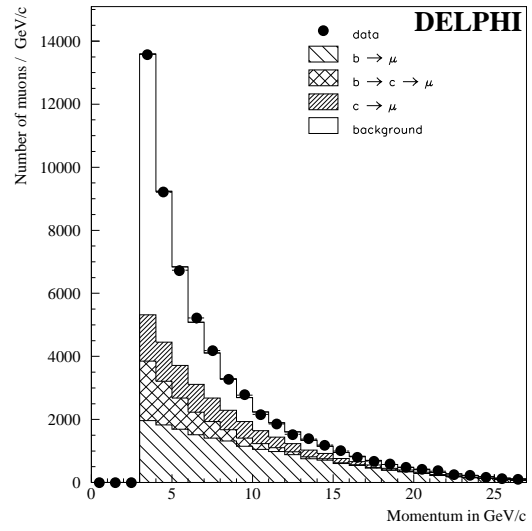


Figure 2: Momentum distribution of muon candidates.

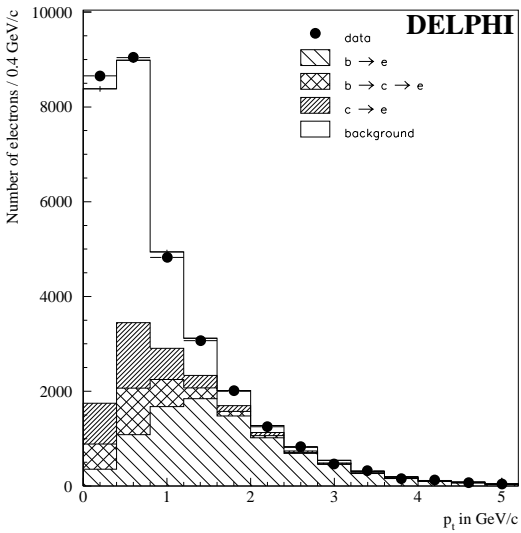


Figure 3: Transverse-momentum distribution of electron candidates.

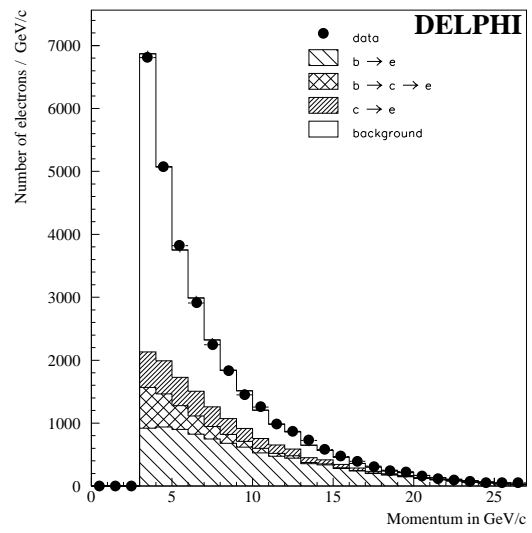


Figure 4: Momentum distribution of electron candidates.

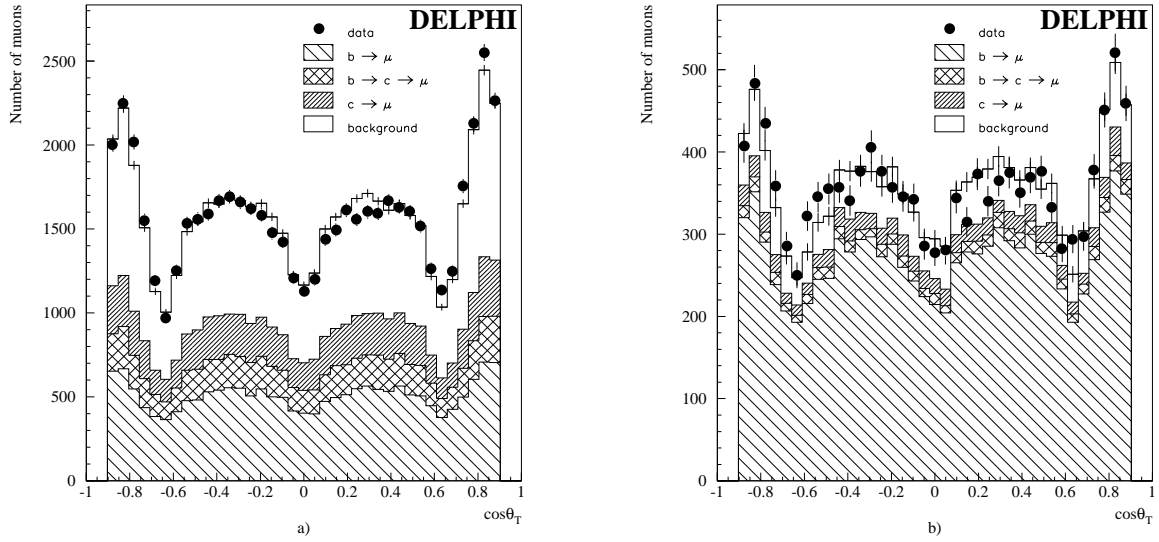


Figure 5: $\cos\theta_T$ distributions for events from the muon sample in the low- and high- p_t regions below a) and above b) 1.6 GeV/c.

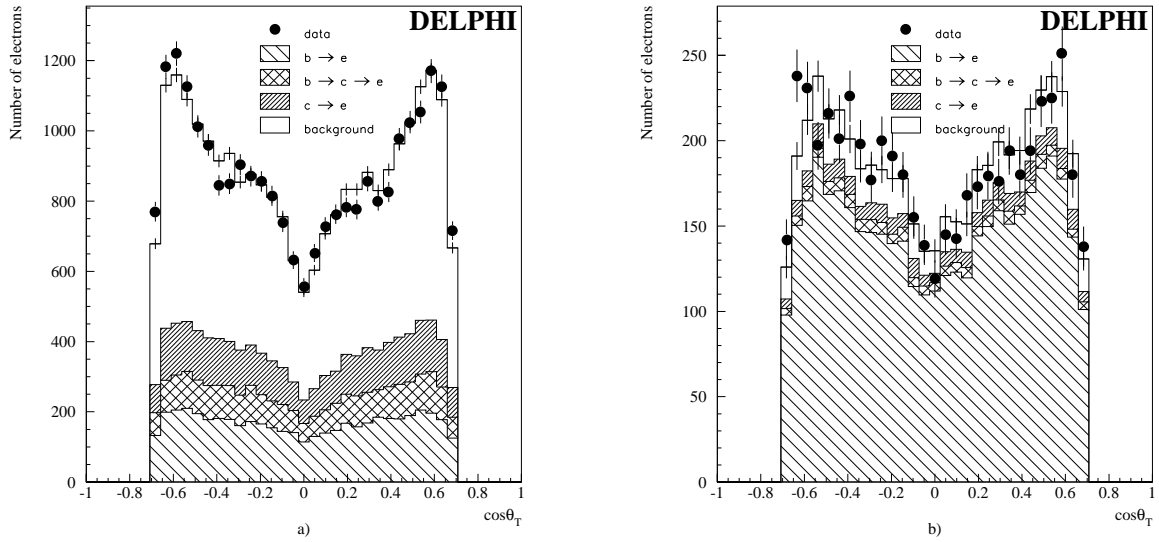


Figure 6: $\cos\theta_T$ distribution for events from the electron sample in the low- and high- p_t regions below a) and above b) 1.6 GeV/c.

3.1.2 Electron sample

Electron candidates were identified by combining the electromagnetic shower information from the HPC with the track ionization measured by the TPC. The probability of the electron hypothesis was computed by comparing the track and shower parameters (momentum-energy, coordinates), monitoring the longitudinal shower development and comparing the energy loss by ionization inside the TPC with the electron hypothesis. To ensure a good detector acceptance and a reasonable background level, candidates were selected with $p > 3 \text{ GeV}/c$ and $0.03 < |\cos \theta_e| < 0.70$. The efficiency of the electron identification for this sample was estimated to be $(56.4 \pm 0.3)\%$ in the simulation.

A sizeable fraction of these electrons originate from photon conversions in the detector. These were discarded by rejecting all track pairs which formed a secondary vertex and whose invariant mass was compatible with zero. The rejection efficiency for these conversion electrons was estimated as 70% and in the simulation only 3% of electrons from b semileptonic decays were rejected. A 20% uncertainty in the number of electrons originating from converted photons and left in the final sample was estimated by a comparison of the data and the simulation in the low- p , low- p_t kinematical domain where this source is dominant.

A study of electrons from Compton and $Z \rightarrow \tau^+ \tau^-$ events showed that the efficiency was lower in the data than in the simulation with a ratio of $(92 \pm 2)\%$ which has been corrected for.

The background was checked with pions from K^0 decay and the probability of misidentification was found to be $(0.60 \pm 0.17)\%$ in the data, compatible with the prediction from the simulation.

A further check of the sample was performed using the two independent means of electron identification provided by the HPC shower measurement and by the track ionization in the TPC, following the method described in reference [13]. A misidentification probability of $(0.59 \pm 0.07)\%$ was obtained.

Taking into account all the selections applied on the electron sample (hadronic selection, track selection, angular and momentum selection), a total identification efficiency of $(23 \pm 1)\%$ was estimated for electrons coming from b semi-leptonic decay. The comparison between the data and the simulation shape for the p and p_t spectra is presented for the electron sample in figures 3 and 4, the $\cos \theta_T$ distribution is in figure 6.

From these studies the relative error on the electron efficiency was estimated to be $\pm 3\%$. The relative error on the contamination from converted photons and mis-identified hadrons was taken to be $\pm 20\%$.

3.2 Lepton sample composition

Several channels lead to leptons in the final state, as shown in table 1.

Processes of the first group in table 1 represent the signal. They give final-state leptons with the same sign as the initial b -quarks and are denoted by the weight f_b .

The total observed asymmetry is given by

$$A_{\text{FB}}^{\text{obs}} = \sum_{x=b, bc, c, bg} f_x \cdot A_{\text{FB}}^x$$

where the fractions f_x associated to each channel depend on the kinematic domain selected. The experimental b -quark asymmetry is then

$$A_{\text{FB}}^{\text{bb}, \text{exp}} = \frac{A_{\text{FB}}^{\text{obs}} - \sum_{x=bc, c, bg} f_x \cdot A_{\text{FB}}^x}{f_b} \quad (2)$$

Type of process "x"	Value of their asymmetry A_{FB}^x	Composition of the samples in %					
		for $l = \mu$			for $l = e$		
		No cut	$p_t > 1.6$	$p_{tin} > 1$	No cut	$p_t > 1.6$	$p_{tin} > 1$
$f_b : b \rightarrow l^-$ $b \rightarrow \tau \rightarrow l^-$ $b \rightarrow \bar{c} \rightarrow l^-$ $b \rightarrow \bar{c} \rightarrow \tau^- \rightarrow l^-$	$A_{\text{FB}}^{\text{bb,exp}}$	31.9	75.3	72.3	29.7	78.8	76.0
$f_{bc} : \bar{b} \rightarrow \bar{c} \rightarrow l^-$ $\bar{b} \rightarrow \bar{c} \rightarrow \tau^- \rightarrow l^-$	$-A_{\text{FB}}^{\text{bb,exp}}$	11.3	3.8	5.7	8.6	3.4	4.9
$f_c : \bar{c} \rightarrow l^-$ $\bar{c} \rightarrow \tau^- \rightarrow l^-$	$-A_{\text{FB}}^{\text{cc}}$	15.1	6.0	4.7	12.0	5.2	4.2
$f_{bg} : \text{Total Background}$	$A_{\text{FB}}^{\text{bg}}$	41.7	14.9	17.3	49.7	12.6	14.9
Number of data candidates		58633	13214	12921	30971	5379	5426

Table 1: Classes definition and composition of the lepton samples in different kinematical domains. (p_{tin} corresponds to the transverse momentum when the lepton is included in the jet. The p_t cuts are in GeV/c).

where f_b is the weighted sum over the first 4 processes of table 1 and $\sum_{x=bc,c,bg} f_x A_{\text{FB}}^x$ is the contribution of the other processes to the observed asymmetry.

Assuming the fixed relation between $A_{\text{FB}}^{\text{cc}}$ and $A_{\text{FB}}^{\text{bb,exp}}$ given by the electroweak couplings in the framework of the Standard Model gives:

$$A_{\text{FB}}^{\text{cc}} = \frac{\lambda}{(1 - 2\chi)} A_{\text{FB}}^{\text{bb,exp}} = c_c A_{\text{FB}}^{\text{bb,exp}}$$

where $(1 - 2\chi)$ is the correction factor which is required to take account of $B_{s(d)}^0 \bar{B}_{s(d)}^0$ mixing. A value of the mixing parameter corresponding to the LEP average [14] of $\chi = 0.115 \pm 0.011$ was used. The error on χ introduced a negligible error (± 0.03) on c_c ($=0.89$) and was therefore neglected. The value of $\lambda = 0.673$ (0.654) was obtained using the program ZFITTER [15] at $\sqrt{s} = 91.28$ (91.23) GeV, corresponding to the mean energy for the 1992 (1991) data sample. For this estimation using the Standard Model, the following values have been considered [16]: Z^0 mass $M_Z = 91.187 \pm 0.007$ GeV/ c^2 , top quark mass $m_{\text{top}} = 166 \pm 16 \pm 19$ GeV/ c^2 , Higgs mass $m_{\text{Higgs}} = 300_{-240}^{+700}$ GeV/ c^2 and QCD coupling constant $\alpha_s = 0.120 \pm 0.006$. The variation of λ as a function of \sqrt{s} was taken into account. The variations on the above Standard Model parameters introduced changes in λ smaller than ± 0.01 and were therefore neglected. This relation introduced in equation (2) gives :

$$A_{\text{FB}}^{\text{bb,exp}} = \frac{A_{\text{FB}}^{\text{obs}} - f_{bg} A_{\text{FB}}^{\text{bg}}}{f_b - f_{bc} - c_c f_c} \quad (3)$$

where $A_{\text{FB}}^{\text{bg}}$ stands for the asymmetry of the background. The coefficients f_b , f_{bc} , f_c , and f_{bg} , are functions of the kinematic domain considered; their estimates depend on the details of the simulation. These coefficients are particularly dependent upon the quantities discussed in the following sections.

Model	$B(b \rightarrow ql^{-}\bar{\nu})$ (%)	$B(b \rightarrow c \rightarrow sl^{+}\nu)$ (%)	Fragmentation	
			$\langle X_E(b) \rangle$	$\epsilon_b \cdot 10^4$
ISGW**	11.5 ± 0.3	7.4 ± 0.5	0.714 ± 0.004	$32 \begin{smallmatrix} + \\ - \end{smallmatrix} \begin{smallmatrix} 5 \\ 4 \end{smallmatrix}$
ACCMM	11.0 ± 0.3	7.9 ± 0.5	0.700 ± 0.004	$50 \begin{smallmatrix} + \\ - \end{smallmatrix} \begin{smallmatrix} 7 \\ 6 \end{smallmatrix}$

Table 2: Branching ratios and fragmentation parameters used in this analysis. These numbers correspond to the mean, extracted in the same way as in [20], of LEP results from [2,21,22].

3.2.1 The fractions of $c\bar{c}$ and $b\bar{b}$ produced in the Z decay

For $\frac{\Gamma_{b\bar{b}}}{\Gamma_{had}}$ and $\frac{\Gamma_{c\bar{c}}}{\Gamma_{had}}$, the Standard Model values of 0.217 ± 0.003 and 0.171 ± 0.014 respectively were taken. The errors correspond to the precision currently reached at LEP on these quantities [16].

3.2.2 The value of the beauty semileptonic branching ratio

The variation of the sample composition as a function of the kinematical cuts is sensitive to the lepton spectra in the B rest frame. Two decay models were considered to study this systematic effect (following the work done by CLEO [17]). The first is based on the ISGW model of Isgur et al [18], with the fraction of D^{**} fixed to 32% as fitted by CLEO [17] (ISGW** model). The second model considered is the one developed by Altarelli et al. [19] (ACCMM model).

The latest LEP results [2,20–22] for the semi-leptonic branching ratio of B decays were used, giving the two sets of numbers quoted in the second column of table 2.

The central value for $A_{FB}^{b\bar{b},exp}$ and $A_{FB}^{c\bar{c}}$ given in this analysis will be the mean of the results corresponding to these two models with a systematic error estimated as half of the difference. For each model, the corresponding set of measured parameters (shown in table 2) were used to take correctly into account the correlations between the different measured parameters.

3.2.3 The relative contribution of leptons from cascade decays

The $b \rightarrow c \rightarrow l^{+}$ branching ratio was extracted from the same LEP analyses as $b \rightarrow l$ [2,20–22]. The LEP averages used in this analysis are quoted in the third column of table 2. From the numbers given by CLEO [17], it is possible (as described in reference [13]) to extract a branching ratio for $b \rightarrow c \rightarrow l^{+}$ of 8.5% and for $b \rightarrow \bar{c} \rightarrow l^{-}$ a value of 0.9%. The errors on these evaluations are large given the extrapolation of the b sample composition from the $\Upsilon(4S)$ to the Z . As no experimental result from LEP is available for $b \rightarrow \bar{c} \rightarrow l^{-}$, the value 0.9% was used with an error of $\pm 0.5\%$.

3.2.4 The value of the charm semileptonic branching ratio

For $c \rightarrow l$ the value of $9.5 \pm 0.9\%$ from ARGUS [23] was used. To describe the lepton spectra in the D decays a fit to the DELCO [24] and MARKIII [25] data was performed with the ACCMM model giving a set of ACCMM parameters, namely the mass (m_s) of the quark produced in the c decay and the Fermi momentum (p_f) of the spectator quark. To take into account the effects of the knowledge of the lepton spectra in the D rest frame, the approach proposed by the LEP-electroweak group [26] was used: two

other sets of ACCMM parameters, corresponding to a one standard deviation variation, were considered to estimate the systematic error and will be used in section 3.4. The same decay model was used for the semi-leptonic decay of the D in the cascade decay $b \rightarrow c/\bar{c} \rightarrow l$.

3.2.5 The hardness of the b and c fragmentation

The Peterson fragmentation function [10] was used for the b -quark with ϵ_b as given in table 2. These values take into account the tuning of the DELPHI simulation, and correspond to the mean energy $\langle X_E(b) \rangle$ taken by a b hadron as measured at LEP. The values used for $\langle X_E(b) \rangle$ (shown in table 2) were extracted from the same LEP analyses [2,21,22] as those used for $b \rightarrow l^-$ and $b \rightarrow c \rightarrow l^+$. For the $e^+e^- \rightarrow Z \rightarrow c\bar{c}$ events the Peterson fragmentation function with $\epsilon_c = 0.064_{-0.012}^{+0.015}$ was used. This value of ϵ_c corresponds to $\langle X_e(D^*) \rangle = 0.495 \pm 0.010$, the mean of the most recent LEP results on D^* production [27-29].

3.3 The χ^2 fit of $A_{\text{FB}}^{\text{bb},\text{exp}}$

A binned fit of the observed charge asymmetry as a function of $\cos \theta_T$ was performed. In each bin i of the space[†] ($\cos \theta_T, p_l, p_t$) an asymmetry was measured :

$$A_{\text{FB}}^{\text{obs},i} = \frac{N^-(i) - N^+(i)}{N^-(i) + N^+(i)}$$

where $N^\pm(i)$ is the number of data events with lepton charge sign $+$ or $-$ in the bin i . A χ^2 minimization was then performed over the bins to obtain the asymmetry $A_{\text{FB}}^{\text{bb},\text{exp}}$. The χ^2 was defined by

$$\chi^2 = \sum_i \frac{\left(A_{\text{FB}}^{\text{bb},\text{exp}} W_{\theta_T}^i - \frac{A_{\text{FB}}^{\text{obs},i} - f_{bg}^i A_{\text{FB}}^{\text{bg},i}}{f_b^i - f_{bc}^i - c_c f_c^i} \right)^2}{\sigma_i^2} \quad (4)$$

where:

- $W_{\theta_T}^i = \frac{8}{3} \frac{1}{n_{\text{data}}^i} \sum_{j=1}^{n_{\text{data}}^i} \frac{\cos(\theta_T^j)}{1 + \cos(\theta_T^j)^2}$ takes into account the θ dependence of the asymmetry.
- σ_i is the error including effects from both data and simulation statistics.
- the other parameters have the same definition as in equation (3). The different f_x^i were determined from the simulation.

The simulation estimates

$$f_{bg} A_{\text{FB}}^{\text{bg}} = f_{bg} \frac{N^{bg,-} - N^{bg,+}}{N^{bg}} = 0.0037 \pm 0.0016 \quad (5)$$

averaged over the full p, p_t spectrum. As noted in section 3.1.1, the simulation predicts a charge correlation between the initial quark and ‘punch-through’ tracks with high p, p_t . For this reason $A_{\text{FB}}^{\text{bg},i}$ must be known in each p, p_t bin. To optimize the estimation of $A_{\text{FB}}^{\text{bg},i}$ in the simulation, the charge correlation between a background track and the initial quark was evaluated and, for each quark species, this correlation was combined with

[†] p_l is the lepton longitudinal momentum defined by $p_l = \sqrt{p^2 - p_t^2}$

the corresponding quark forward-backward asymmetry. The Standard Model forward-backward asymmetries for the different quark species have been estimated by ZFITTER with the same parameters as in section 3.2. The background asymmetry can be written

$$A_{\text{FB}}^{\text{bg},i} = \sum_q W_{\theta_T}^i \frac{n_{\text{bg},i}^q}{n_{\text{bg},i}} A_{\text{FB}}^{\text{qq}} S_{\text{bg},i}^q \quad (6)$$

where:

- \sum_q stands for the sum over the different quark species.
- $S_{\text{bg},i}^q = \frac{n_{\text{bg},i,\text{like sign}}^q - n_{\text{bg},i,\text{unlike sign}}^q}{n_{\text{bg},i}^q}$, where $n_{\text{bg},i,x}^q$ is the number of background particles with the same or opposite charge sign as the initial quark.

For a given simulated sample the precision reached on $A_{\text{FB}}^{\text{bg},i}$ with equation (6) is improved by a factor ~ 10 in comparison with that from equation (5), as no statistical error has to be considered on $A_{\text{FB}}^{\text{q}\bar{\text{q}}}$. The results obtained are listed in table 3.

Kinematical domain	$f_{\text{bg}} A_{\text{FB}}^{\text{bg}}$
Full sample	0.0024 ± 0.0001
$8 > p > 3 \text{ GeV}/c$ and $p_t < 1 \text{ GeV}/c$	0.0028 ± 0.0002
$p > 8 \text{ GeV}/c$ and $p_t < 1 \text{ GeV}/c$	0.0048 ± 0.0004
$p > 3 \text{ GeV}/c$ and $p_t > 1.6 \text{ GeV}/c$	0.0019 ± 0.0001

Table 3: Background contribution to the observed asymmetry as estimated by simulation using equation (6) for different kinematical domains.

The μ and e data sets have been split according to the year of data taking to allow for changes in the detector. For each of these four samples the binning was adapted to obtain ~ 200 events per data bin. A negligible dependence of the result with the number of bins in $\cos \theta_T, p_l, p_t$ was observed. When the bin size is too wide in p_t the precision of the result deteriorates, as the leptons from b -quark decay are not so well separated from the other leptonic classes. The minimization of the χ^2 was performed on the four samples simultaneously.

The measured asymmetry was:

$$A_{\text{FB}}^{\text{b}\bar{\text{b}},\text{exp}} = 0.080 \pm 0.010(\text{stat.}) \left(\frac{\chi^2}{d.o.f.} = \frac{414}{409} \right).$$

The corresponding $A_{\text{FB}}^{\text{b}\bar{\text{b}},\text{exp}}$, obtained for different $|\cos \theta_T|$ values, is shown figure 7 and its stability as a function of different kinematical cuts is shown figure 8. The mean LEP energy corresponding to the selected sample is 91.27 GeV. The values obtained independently for the different samples can be found in table 4.

Other fitting methods were applied to the samples: an unbinned likelihood fit and a χ^2 fit to the $\cos \theta_T$ distribution of the events in the high- p_t region. In addition, in a separate multivariate analysis [30], two other variables (the fraction of the jet momentum carried by the lepton and the angle between the lepton and the closest charged-particle track

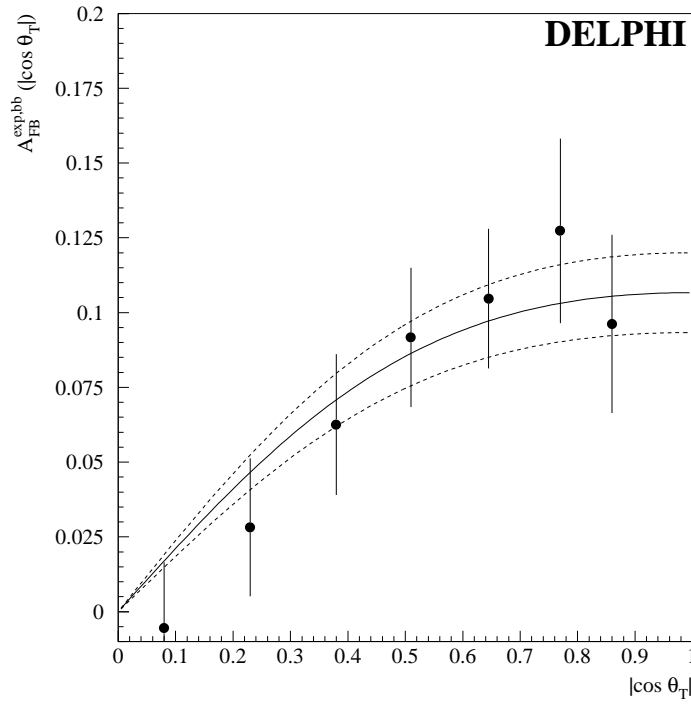


Figure 7: Observed values of $A_{\text{FB}}^{\text{bb,exp}}(x) = A_{\text{FB}}^{\text{bb,exp}} \frac{8}{3} \frac{x}{1+x^2}$ for different $x = |\cos \theta_T|$. Full curve: χ^2 fit; dashed curves: one standard deviation from the central value; data points: observed asymmetries at the center of the $\cos \theta_T$ bin.

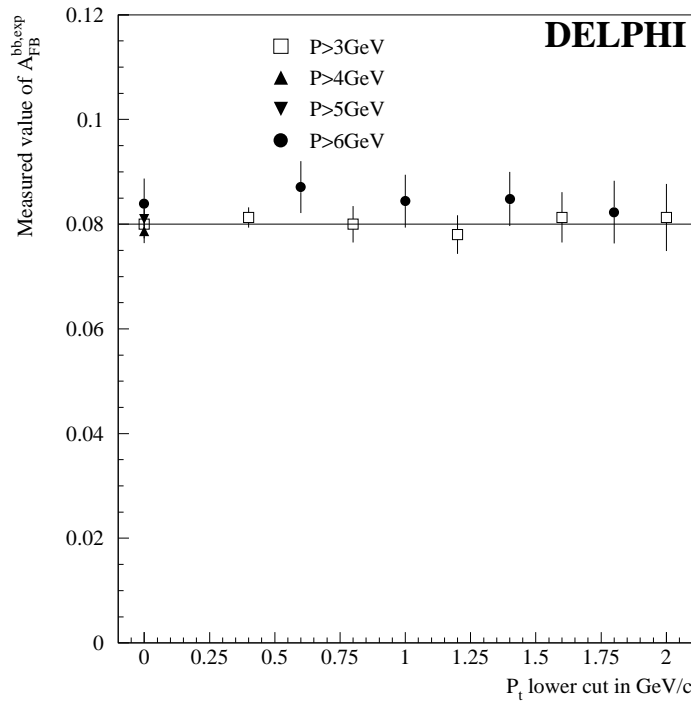


Figure 8: Measured values of $A_{\text{FB}}^{\text{bb,exp}}$ for various values of the p cut as a function of the p_t cut. The reference line is drawn from the point $p > 3$ GeV/c, no p_t cut.

Sample	$A_{\text{FB}}^{\text{bb},\text{exp}}$	$\frac{\chi^2}{d.o.f.}$
μ 1992 only	0.084 ± 0.012	233/223
e 1992 only	0.068 ± 0.022	88/89
μ 1991 only	0.081 ± 0.026	58/55
e 1991 only	0.083 ± 0.040	35/39
All samples	0.080 ± 0.010	414/409

Table 4: Results of the 1-parameter fit to $A_{\text{FB}}^{\text{bb},\text{exp}}$ and the corresponding value of the χ^2 per degree of freedom for the different samples. The mean LEP energies were 91.28 GeV and 91.23 GeV for 1992 and 1991 respectively.

with momentum above 1 GeV/c) were combined with p and p_t to improve the separation between leptons from $b \rightarrow l$ and leptons from other sources. All of these approaches gave compatible results within their statistical and systematical accuracy. The results obtained with the binned χ^2 fit are quoted in table 4. This method was chosen since it gives a good compromise between the statistical precision reached and the amount of input needed for the description of the sample composition.

A two-parameter fit was also performed to measure $A_{\text{FB}}^{\text{bb},\text{exp}}$ and $A_{\text{FB}}^{\text{cc}}$ simultaneously, giving:

$$\begin{aligned}
 A_{\text{FB}}^{\text{bb},\text{exp}} &= 0.080 \pm 0.010(\text{stat.}) \\
 A_{\text{FB}}^{\text{cc}} &= 0.083 \pm 0.022(\text{stat.}) \\
 \frac{\chi^2}{d.o.f.} &= \frac{413}{408}
 \end{aligned}$$

with a statistical correlation of 0.27 between the two parameters.

3.4 Systematic uncertainties

3.4.1 Production and Decay models of b and c quarks

The parameters involved in the determination of the composition fractions f_x were varied as described in section 3.2.

The dependence on the lepton spectrum model in $b \rightarrow l$ decay was computed by considering the ISGW** and ACCMM models with the corresponding measured branching ratio and fragmentation (shown in table 2). The half difference between the results obtained with these two models was used as an estimate of the ‘ b -quark decay model’ systematic uncertainty and the mean used in the derivation of the quoted asymmetry. The results for the different models are shown in table 5.

The part of the systematic error reflecting the current precision on the parameters of b - and c -quarks production and decay was ± 0.0021 . This number corresponds to the top part of table 6.

3.4.2 Lepton identification and background

As explained in section 3.1, the lepton efficiency and the contamination were varied independently. Due to the method developed to extract the asymmetries, the sensitivity to the efficiency was negligible. A correlation between the background values in the 1991

Model	$A_{\text{FB}}^{\text{b}\bar{\text{b}},\text{exp}}$	Two-parameter fit	
		$A_{\text{FB}}^{\text{b}\bar{\text{b}},\text{exp}}$	$A_{\text{FB}}^{\text{c}\bar{\text{c}}}$
ACCMM	0.0806 ± 0.0096	0.0801 ± 0.0097	0.0801 ± 0.0225
ISGW**	0.0801 ± 0.0096	0.0794 ± 0.0097	0.0861 ± 0.0222
Mean	0.080 ± 0.010	0.080 ± 0.010	0.083 ± 0.022

Table 5: Results for $A_{\text{FB}}^{\text{b}\bar{\text{b}},\text{exp}}$ and $A_{\text{FB}}^{\text{c}\bar{\text{c}}}$ for the different b decay models.

and 1992 samples can be expected. The contamination was therefore varied at the same time for both data sets. The variation of the background and efficiency by the amounts given in section 3.1 changed the asymmetry by ± 0.0019 .

3.4.3 Background asymmetry

The contribution of the background to the observed asymmetry was estimated from the simulation. Due to a cancellation between the kinematical domains, dominated in one instance by leptons from charm semi-leptonic decays and in the other by leptons from beauty semi-leptonic decays, the background asymmetry introduced a correction of only ~ 0.0009 to $A_{\text{FB}}^{\text{b}\bar{\text{b}},\text{exp}}$ in the one parameter fit. The background correlated in charge with the initial quark was high in the kinematical region where charm decays were important (intermediate p, p_t), therefore the impact on the measured charm asymmetry was large. To estimate the systematic error coming from this correction, the background asymmetry obtained from the simulation was varied by $\pm 50\%$.

3.4.4 Reconstruction effects, binning

The systematic error coming from the thrust axis reconstruction was estimated using the simulation. The effect was found to be lower than 0.0007. To completely describe the charged-track and neutral-cluster energy a slight smearing was applied in the simulation. The corresponding changes in the p_t reconstruction induced variations of ± 0.0007 on $A_{\text{FB}}^{\text{b}\bar{\text{b}},\text{exp}}$.

To check the stability of the method, the number of events per bin was varied between 80 and 300 and, for a given number of events per bin, the bin boundaries were changed. The observed change was considered as the systematic uncertainty due to the variation of the sample composition resulting from the bin definition.

3.5 Final result of the lepton analysis

Combining the 1991 and 1992 DELPHI lepton samples gave the result:

$$A_{\text{FB}}^{\text{b}\bar{\text{b}},\text{exp}} = 0.080 \pm 0.010(\text{stat.}) \pm 0.003(\text{syst.}).$$

To obtain the final value of the $b\bar{b}$ forward-backward asymmetry, the value of $A_{\text{FB}}^{\text{b}\bar{\text{b}},\text{exp}}$ must be corrected for the mean $B_{s(d)}^0 \bar{B}_{s(d)}^0$ mixing found at LEP: $\chi = 0.115 \pm 0.009 \pm 0.006$ [14], which yields:

$$A_{\text{FB}}^{\text{b}\bar{\text{b}}} = 0.104 \pm 0.013(\text{stat.}) \pm 0.004(\text{syst.}) \pm 0.003(\text{mixing}).$$

Changed parameters	Central value	Variations applied	Fit of	Two-parameter fit	
			$A_{FB}^{b\bar{b},\text{exp}}$	$A_{FB}^{b\bar{b},\text{exp}}$	$A_{FB}^{c\bar{c}}$
b decay model	<ACCMM, ISGW** >	ACCMM, ISGW**	± 0.0003	± 0.0003	∓ 0.0027
c decay model	$m_s = 1 \text{ MeV}$ $p_f = 467 \text{ MeV}$	$^{+153}_{-0} \text{ MeV}$ $^{+0}_{-114} \text{ MeV}$	± 0.0014	± 0.0014	∓ 0.0013
$Br(b \rightarrow l)$	0.113	± 0.0034	∓ 0.0009	∓ 0.0009	± 0.0015
$Br(b \rightarrow c \rightarrow l)$	0.077	± 0.005	± 0.0002	± 0.0002	∓ 0.0025
$Br(b \rightarrow \bar{c} \rightarrow l)$	0.009	± 0.005	± 0.0005	± 0.0005	± 0.0038
$Br(c \rightarrow l)$	0.095	± 0.009	± 0.0004	± 0.0006	∓ 0.0067
$\Gamma_{b\bar{b}}/\Gamma_{had}$	0.217	± 0.003	∓ 0.0003	∓ 0.0003	± 0.0004
$\Gamma_{c\bar{c}}/\Gamma_{had}$	0.171	± 0.014	± 0.0006	± 0.0007	∓ 0.0053
ϵ_b	0.004	± 0.0006	± 0.0001	± 0.0001	± 0.0005
ϵ_c	0.064	± 0.015	∓ 0.0007	∓ 0.0008	± 0.0001
background and efficiency for Muons		$\pm 15 \%$ $\mp 3 \%$	± 0.0016	± 0.0015	± 0.0051
background and efficiency for electrons		$\pm 20 \%$ $\mp 3 \%$	± 0.0011	± 0.0011	± 0.0025
background asymmetry		$\pm 50 \%$	∓ 0.0004	∓ 0.0009	± 0.0102
p_t and thrust reconstruction			± 0.0010	± 0.0010	± 0.0009
sample binning			± 0.0010	± 0.0010	± 0.0045
total			0.003	0.003	0.016

Table 6: Different contributions to the systematic error in the χ^2 fit of the lepton sample. The estimated correlation between the systematics of $A_{FB}^{c\bar{c}}$ and $A_{FB}^{b\bar{b},\text{exp}}$ in the two-parameter fit is -0.07.

The value of $A_{\text{FB}}^{\text{c}\bar{\text{c}}}$ obtained from the lepton sample is:

$$A_{\text{FB}}^{\text{c}\bar{\text{c}}} = 0.083 \pm 0.022(\text{stat.}) \pm 0.016(\text{syst.}).$$

The total correlation between $A_{\text{FB}}^{\text{c}\bar{\text{c}}}$ and $A_{\text{FB}}^{\text{b}\bar{\text{b}}}$ in the two-parameter fit (considering the statistical, systematical and mixing errors) was 0.19. The $A_{\text{FB}}^{\text{b}\bar{\text{b}}}$ value and errors, at the precision given here, were the same for the one- and the two-parameter fits.

4 $A_{\text{FB}}^{\text{b}\bar{\text{b}}}$ measurement using a lifetime tag

In this section a measurement of $A_{\text{FB}}^{\text{b}\bar{\text{b}}}$ is presented which is based on an inclusive lifetime tag of B-hadrons. Because of the finite lifetime of such hadrons, charged particles originating from their decay have large impact parameters. This quantity was defined as the distance δ of closest approach between the charged-particle track and the Z production point. δ was given a positive sign if the particle intersected the jet axis in front of the interaction point along the jet direction and a negative sign otherwise. In the present analysis the event vertex, defined as the point from which primary particles emerge, was fitted on an event-by-event basis [31] and was assumed to represent the Z production point. Best sensitivity to lifetime effects was obtained using the significance S , defined as the ratio between δ and its estimated error. This approach allowed an almost totally inclusive tag of $b\bar{b}$ events, because δ depended mainly on the lifetime rather than on other B-hadron production and decay features, such as fragmentation, B-hadron spectroscopy and decay modes.

The Vertex Detector provided a very precise measurement of δ in the plane perpendicular to the colliding beams. Charged-particle tracks produced in the primary interaction had a non-zero impact parameter due only to resolution effects with positive or negative values being equally likely, while the decay products of long lived hadrons mostly had positive values of δ . The negative part of the impact parameter distribution was therefore assumed to be due to experimental resolution effects. The analysis was performed for events having $|\cos\theta_T| \leq 0.70$ in order to match the acceptance of the Vertex Detector, and all efficiencies in the following will be referred to this angular region.

For this inclusive approach, the determination of the charge of the parent quark was not as direct as in the leptonic analysis. A statistical reconstruction of the charge of the original fermion was performed by using a jet-charge algorithm in the two event hemispheres, defined by the plane perpendicular to the thrust axis at the Z production point.

The analysis based on this method used the data collected by the DELPHI experiment during 1992. The different parts of the analysis described are the tag of $b\bar{b}$ events, the determination of the hemisphere charge and the extraction of the forward-backward asymmetry.

4.1 B Enrichment

The probability method originally proposed by ALEPH [32] was used for the enrichment of b-flavour events in hadronic decays of Z . It was assumed that the negative part of the significance distribution did not contain any lifetime information and was therefore representative of the experimental resolution. The significance probability density function $f(S)$ for primary charged-particle tracks was then obtained by symmetrizing

the negative part of the S distribution. The probability $F(S_0)$ that a single track with $S > S_0$ has originated from the primary vertex is:

$$F(S_0) = \int_{S>S_0} f(S)dS$$

By definition, $F(S_0)$ has a flat distribution for primary charged particles while for particles from the secondary vertices the distribution $F(S_0)$ peaks at low probabilities.

For a group of N tracks with positive significance, a tagging variable F_E^+ was defined as follows:

$$F_E^+ \equiv \Pi \cdot \sum_{j=0}^{N-1} (-\ln \Pi)^j / j!, \text{ where } \Pi \equiv \prod_{i=1}^N F(S_i). \quad (7)$$

F_E^+ represented the probability that for this group all particles were produced at the primary interaction point. This variable behaves as a cumulative probability with a flat distribution between 0 and 1, provided all tracks used are uncorrelated. Figure 9 shows the distributions of F_E^+ for different flavours in simulated events. The distribution of F_E^+ for light quarks is approximately flat, while for b -quarks it has a sharp peak at low values. In the construction of the resolution function described above, $f(S)$, the anti- b cut $F_E^+ > 0.1$ was used to suppress the residual contribution of tracks from the decays of B-hadrons. Detailed studies on simulated events showed that this cut reduced the fraction of b -events in the sample to 6.5 %.

B -enrichment could be achieved by selecting events in which samples of charged-particle tracks with positive significance yielded low-probability values, computed using (7). In this analysis two probabilities F_H were obtained for each event using separately the particles in the two hemispheres. The event was selected if, at least in one hemisphere, F_H was lower than a given cut. The B purity P_B was defined as the fraction of $b\bar{b}$ events in the selected sample, and the B efficiency E_B was the probability of selecting a $b\bar{b}$ event with this enrichment procedure. Both the purity and the efficiency were derived using data, by counting the number of selected hemispheres (N_1) and the number of events in which at least one hemisphere was selected (N_2) for a given F_H cut, then the following equations were written:

$$\begin{cases} N_1/(2N_{tot}) &= R_{b\bar{b}} \epsilon_b + R_{q\bar{q}} \epsilon_q \\ N_2/N_{tot} &= R_{b\bar{b}} \epsilon_b (2 - \rho_b \epsilon_b) + R_{q\bar{q}} \epsilon_q (2 - \rho_q \epsilon_q) \end{cases} \quad (8)$$

where:

- N_{tot} was the total number of selected hadronic events;
- $R_{b\bar{b}}$ and $R_{q\bar{q}}$ were the fractions of $b\bar{b}$ and non- $b\bar{b}$ events respectively after hadronic event selection: they were evaluated using simulated events and the value of $\Gamma_{b\bar{b}}$ used in the lepton analysis;
- ϵ_b (ϵ_q) was the probability to tag a hemisphere for a $b\bar{b}$ (non- $b\bar{b}$) event;
- the conditional probability ϵ'_b to tag a hemisphere when the other has been tagged was expressed in terms of the coefficients ρ_b (ρ_q) for a $b\bar{b}$ (non- $b\bar{b}$) event as $\epsilon'_b = \epsilon_b \rho_b$.

For simplicity all non- $b\bar{b}$ events were grouped into one single category. This approximation, quite crude for $c\bar{c}$ events, was nevertheless sufficient for the purposes of this analysis. In this notation the purity and efficiency per event of the B -enrichment were given by:

$$\begin{cases} P_B &= N_{tot} R_{b\bar{b}} \epsilon_b (2 - \rho_b \epsilon_b) / N_2 \\ E_B &= \epsilon_b (2 - \rho_b \epsilon_b). \end{cases}$$

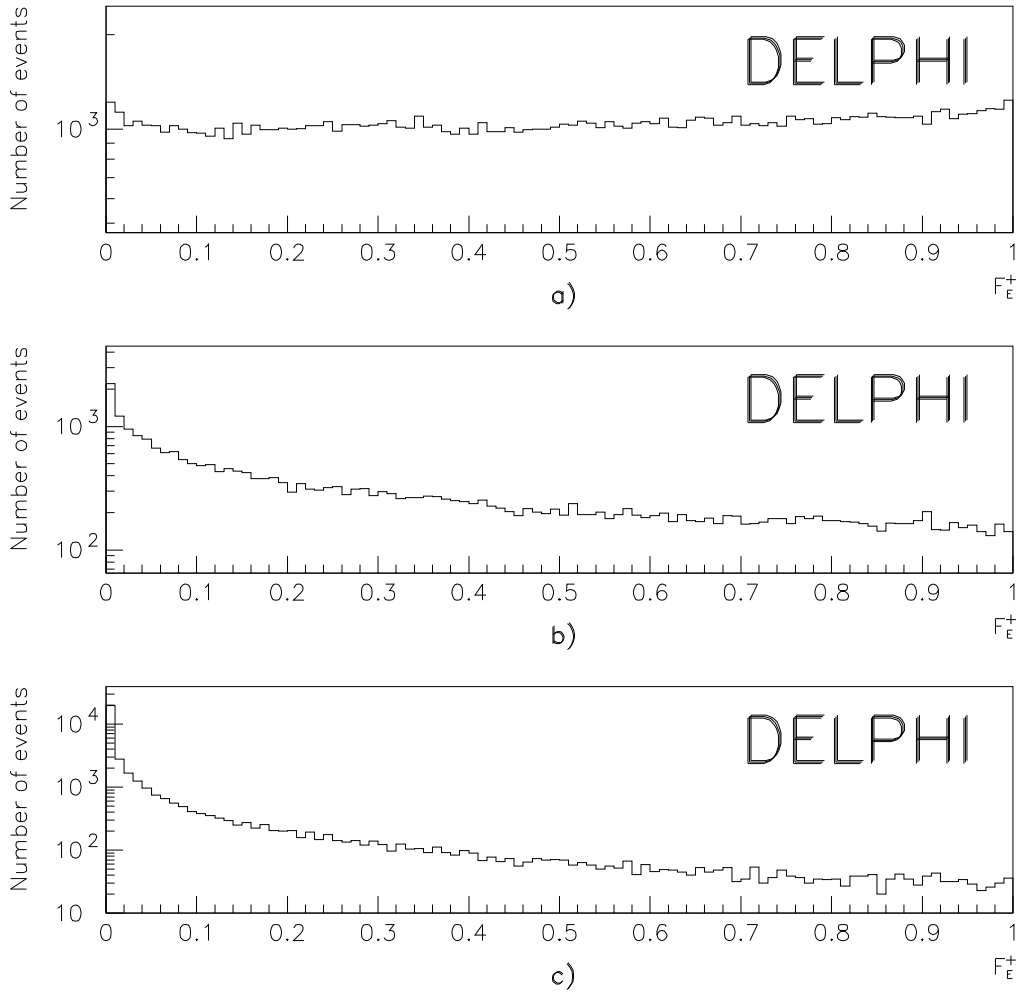


Figure 9: Event probability in simulated events F_E^+ for tracks with positive significance for a) light quark events, b) charm-quark events and c) b -quark events.

The values of E_B and P_B were evaluated from data in a way which minimized the dependence on simulation. Two different methods were followed to solve the equations (8):

- (a) ρ_q and ϵ_q were taken from simulation and ρ_b and ϵ_b were considered as unknowns;
- (b) ρ_b and ρ_q were taken from simulation and ϵ_b and ϵ_q were considered as unknowns.

This procedure was repeated for several values of the cut on F_H and the results are reported in Table 7. For each choice of F_H , the P_B and E_B values obtained from the two methods were averaged and their half-difference was taken as the systematic uncertainty. The corresponding statistical error and the additional uncertainties due to experimental errors on Z hadronic partial widths were evaluated and are negligible.

	method (a)		method (b)	
F_H cut	P_B	E_B	P_B	E_B
0.100	0.556	0.775	0.433	0.663
0.010	0.795	0.442	0.740	0.417
0.007	0.814	0.379	0.784	0.367
0.003	0.830	0.279	0.861	0.269

Table 7: B Purity and B efficiency of the tag for different values of the F_H cut.

The selection $F_H < 0.01$ was found to give the best compromise between efficiency and purity for the measurement of $A_{FB}^{b\bar{b}}$ and was used for the present analysis. It corresponded to $P_B = 0.77 \pm 0.03$ and $E_B = 0.43 \pm 0.01$. The non b flavours were assumed to be in the proportion predicted by Monte Carlo simulation. The sample composition after B enrichment is shown in Table 8.

Event type	P_f
$u\bar{u}$	0.04 ± 0.01
$d\bar{d}$	0.04 ± 0.01
$s\bar{s}$	0.04 ± 0.01
$c\bar{c}$	0.11 ± 0.01
$b\bar{b}$	0.77 ± 0.03

Table 8: Composition of the tagged sample for $F_H < 0.01$.

4.2 The hemisphere charge determination

The quark charge was identified by means of the jet charge variable [33], which partly retains the quark charge information in hadronic events. The two hemisphere jet charges were defined as:

$$Q_F = \frac{\sum_i q_i |\vec{p}_i \cdot \vec{T}|^k}{\sum_i |\vec{p}_i \cdot \vec{T}|^k}, \quad \vec{p}_i \cdot \vec{T} > 0$$

$$Q_B = \frac{\sum_i q_i |\vec{p}_i \cdot \vec{T}|^k}{\sum_i |\vec{p}_i \cdot \vec{T}|^k}, \quad \vec{p}_i \cdot \vec{T} < 0$$

where \vec{T} was the thrust unit vector, q_i the particle charge, \vec{p}_i the particle momentum and the exponent k is a positive number. $Q_{F(B)}$ referred to the forward (backward) hemisphere. To ensure good charge sensitivity, events were accepted only if they:

- did not contain any charged particle with reconstructed momentum $> 50 \text{ GeV}/c$;
- had at least 4 reconstructed charged-particle tracks both in the forward and in the backward hemispheres;
- had a sum of reconstructed charged-particle momenta greater than $3 \text{ GeV}/c$ in each hemisphere separately.

As described in [34], a weighting technique, not relying on the simulation, was applied to the jet charge algorithm to compensate for the excess of positively charged particles induced by secondary interactions of hadrons with matter.

The b -quark direction was approximated with the thrust axis. As the charge of the b -quark is negative, the hemisphere with lower jet charge was assigned to it. Simulated events were used to study the probability C_b that this orientation of the b -quark was correct. Using simulation the value of the exponent k was tuned to optimize the probability C_b of correct charge assignment in $b\bar{b}$ events: $k = 0.5$ was chosen. The hemisphere charge distributions for data and simulated events are shown in figure 10(a). The disagreement between the width of the two distributions amounts to less than 1.5% and was verified to have no effect in the present analysis. The stability of C_b with respect to $|\cos\theta_T|$ was studied on simulated events and the variation of C_b as a function of $|\cos\theta_T|$ is shown in figure 10(b). No significant variation is observed over the range $|\cos\theta_T| < 0.70$. Table 9 summarizes the C_f for the different quark types ($f = u, d, s, c, b$) obtained with simulated events.

Event type	C_f
$u\bar{u}$	0.756 ± 0.002
$d\bar{d}$	0.700 ± 0.002
$c\bar{c}$	0.652 ± 0.002
$s\bar{s}$	0.701 ± 0.002
$b\bar{b}$	0.689 ± 0.002
$b\bar{b}$ from data	0.673 ± 0.012

Table 9: The probabilities C_f ($f = u, d, s, c, b$) obtained from simulated events. For $b\bar{b}$ events the value obtained from the data, as described in the text, is also reported.

The probabilities C_f depend on several physical parameters of the simulation which are known with large uncertainties. This could give large systematic errors on $A_{\text{FB}}^{b\bar{b}}$. Therefore C_b was measured from the data themselves and only $C_{f \neq b}$ were derived from simulation, their effect on the measurement being limited by the B -enrichment procedure. The determination of C_b was based on the lepton sample of the previous analysis. For each selected lepton, the jet charge in the opposite hemisphere was considered. Two hemisphere charge distributions were built up: Q_{l+} opposite to positive leptons and Q_{l-} to negative ones. The leptonic sample was composed of the following categories:

1. direct or cascade b (\bar{b}) quark decays to a lepton or misidentified hadron of negative (positive) charge;
2. direct or cascade b (\bar{b}) quark decays to a lepton or misidentified hadron of positive (negative) charge;
3. direct or cascade \bar{c} (c) quark decays to a lepton or misidentified hadron of negative (positive) charge;
4. \bar{c} (c) quark decays to a misidentified hadron of positive (negative) charge;
5. misidentifications in uds events with correct charge correlation;

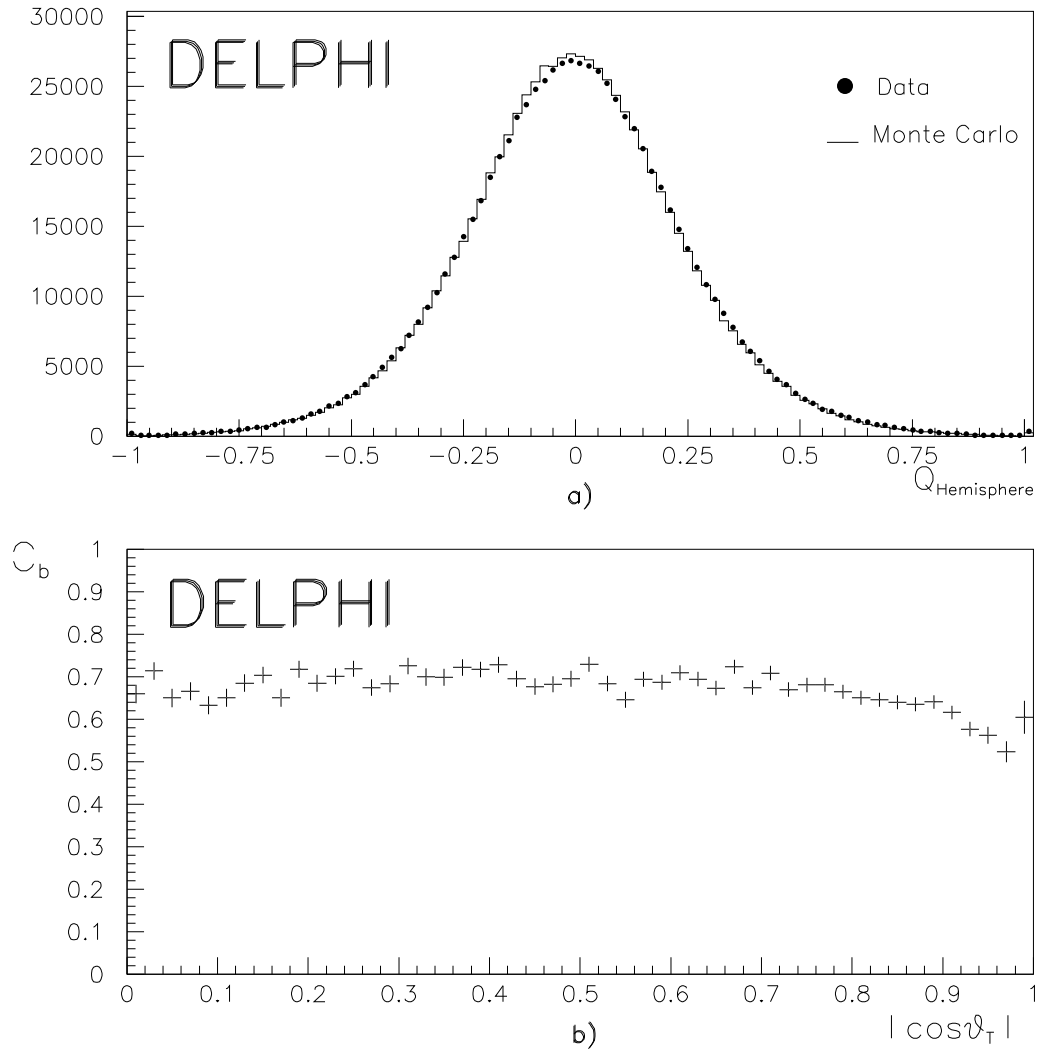


Figure 10: a) Hemisphere charge distributions Q_H for data and simulated events, and b) Variation of C_b with $|\cos\theta_T|$.

6. misidentifications in uds events with wrong charge correlation;

Therefore $Q_{l\pm}$ could be written as:

$$\begin{cases} Q_{l+} = [(1 - \chi)f_1 + \chi f_2] Q_b + [(1 - \chi)f_2 + \chi f_1] Q_{\bar{b}} + \\ \quad + f_3 Q_{\bar{c}} + f_4 Q_c + f_5 Q_{uds}^- + f_6 Q_{uds}^+ \\ Q_{l-} = [(1 - \chi)f_2 + \chi f_1] Q_b + [(1 - \chi)f_1 + \chi f_2] Q_{\bar{b}} + \\ \quad + f_3 Q_c + f_4 Q_{\bar{c}} + f_5 Q_{uds}^+ + f_6 Q_{uds}^- \end{cases} \quad (9)$$

where $f_{i,i=1,6}$ indicates the relative fraction of category i , $\chi = 0.115 \pm 0.011$ is the average mixing parameter at LEP [14]. The equations (9) could be inverted to give $Q_{b(\bar{b})}$ from which C_b was derived. The hemisphere charge distributions $Q_{c(\bar{c})}$, Q_{uds}^\pm were derived from simulation as well as the fractions f_i of lepton sample composition. By varying the cut on the p_t of the selected lepton different compositions could be achieved. The distributions $Q_{b(\bar{b})}$ obtained from the muon sample with $p_t > 1.6$ GeV/c are shown in figure 11(a).

In principle a correction factor c_{tag} should be applied to take into account the decrease of C_b in the B -enriched sample because the lifetime tag selected higher decay times, thus increasing the fraction of mixed B -hadrons. The effect was studied with simulated events and no significant change was observed. The lepton sample with $p_t > 1.6$ GeV/c was found to give the best compromise between statistical and systematic uncertainty, the result was:

$$\begin{aligned} C_b &= 0.665 \pm 0.014(stat.) \quad (muon \ sample) \\ C_b &= 0.686 \pm 0.018(stat.) \quad (electron \ sample) \end{aligned}$$

As a consistency check the probability C_b was also evaluated for different p_t intervals of the leptonic sample. The results obtained separately with the muon and the electron samples are shown in figure 11(b).

The systematic uncertainties on the C_b determination reflect mainly the uncertainties on the lepton sample composition, as in the previous analysis. The detailed list is shown in table 10. The shape of the hemisphere-charge distributions of the backgrounds depended on several physical parameters, the only significant effect was obtained varying the Peterson fragmentation parameter for $c\bar{c}$ events in the above described interval. The effect of the uncertainty on the average mixing parameter χ was also derived. Finally a systematic uncertainty was estimated for the correction c_{tag} . The contribution was evaluated by varying the B_d^0 mixing parameter within its experimental uncertainty [35]. The sources of systematic uncertainties are shown in table 10. The final value after combining muons and electrons results was

$$C_b = 0.673 \pm 0.011(stat.) \pm 0.003(syst.) \pm 0.005(mixing).$$

4.3 Results

The total sample of hadronic events collected during 1992 was subjected to the event selection, B -enrichment and hemisphere-charge determination. The charge-signed angular distribution for selected events was corrected for the angular acceptance of the microvertex detector by using the fraction of selected events as function of the $|\cos\theta_T|$, which is shown in figure 12. This angular distribution was parameterised with a 4-degree polynomial function and the result of the fit is shown on the same figure. The experimental $\cos\theta_T$ distribution was signed assuming that the lower (higher) hemisphere charge

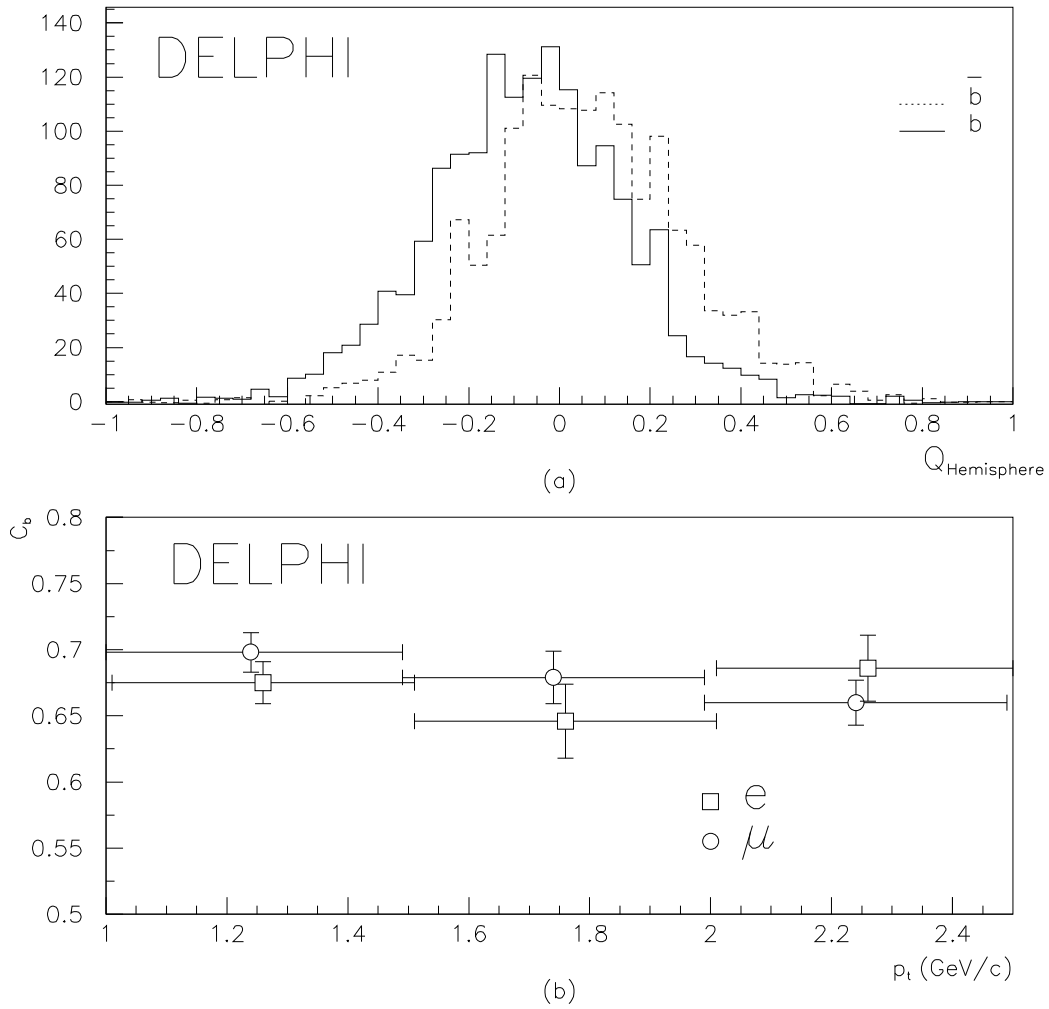


Figure 11: a) Hemisphere charge distributions, $Q_{b(\bar{b})}$, as obtained from the data for the muon sample with $p_t > 1.6$ GeV/c. b) The probability C_b for different p_t intervals, only statistical errors are reported.

Source of uncertainty	ΔC_b
Variation of $Br(b \rightarrow l)$	∓ 0.001
Variation of $Br(b \rightarrow c \rightarrow l)$	$< 5 \cdot 10^{-4}$
Variation of $Br(b \rightarrow \bar{c} \rightarrow l)$	± 0.001
Variation of $Br(c \rightarrow l)$	$< 5 \cdot 10^{-4}$
Modelling of $b \rightarrow l$ decay	$< 5 \cdot 10^{-4}$
Modelling of $c \rightarrow l$ decay	$< 5 \cdot 10^{-4}$
Variation of $\Gamma_{b\bar{b}}/\Gamma_{had}$	$< 5 \cdot 10^{-4}$
Variation of $\Gamma_{c\bar{c}}/\Gamma_{had}$	$< 5 \cdot 10^{-4}$
Variation of ϵ_b	$< 5 \cdot 10^{-4}$
Variation of ϵ_c	$< 5 \cdot 10^{-4}$
Variation of the background/efficiency for leptons	± 0.002
$Q_c, Q_{\bar{c}}$ jet charge distribution	∓ 0.001
c_{tag} correction for lifetime tag	∓ 0.001
χ experimental uncertainty	± 0.005

Table 10: Systematic error contributions to C_b measurement. Uncertainty sources common with table 6 have the same central values and the same excursions of the parameters.

corresponded to the negatively (positively) charged fermion, namely:

$$\cos\Theta = -\text{sign}(Q_F - Q_B) \cdot \cos\theta_T,$$

and the final distribution of $\cos\Theta$ is shown in figure 13.

A χ^2 -fit was performed on this distribution over the angular region $|\cos\Theta| \leq 0.70$, to evaluate, according to equation (1), the asymmetry parameter. The result was:

$$A_{FB}^{B-tag} = (3.02 \pm 0.46)\%, \quad \text{Prob}(\chi^2) = 0.09.$$

The observed forward-backward asymmetry of the B -enriched sample, A_{FB}^{B-tag} , was a linear superposition of single $A_{FB}^{f\bar{f}}$ asymmetries weighted with the relative B -enrichment compositions P_f . The up quarks and $down$ quarks contributed with opposite sign to the observed asymmetry. Furthermore the probabilities C_f reduced the original $A_{FB}^{f\bar{f}}$ by a factor $(2C_f - 1)$ and the experimental observed asymmetry was expressed as:

$$A_{FB}^{B-tag} = \sum_f \text{sign}(-q_f) P_f (2C_f - 1) A_{FB}^{f\bar{f}}.$$

The asymmetry for b -quarks was then extracted assuming the relations $A_{FB}^{c\bar{c}} = A_{FB}^{u\bar{u}}$ and $A_{FB}^{b\bar{b}} = A_{FB}^{d\bar{d}} = A_{FB}^{s\bar{s}}$, which in the Standard Model are violated by $b\bar{b}$ vertex corrections which are much smaller than the presently obtainable experimental uncertainties. Putting $A_{FB}^{c\bar{c}} = \lambda A_{FB}^{b\bar{b}}$ the following expression was obtained:

$$A_{FB}^{b\bar{b}} = \frac{A_{FB}^{B-tag}}{P_b(2C_b - 1) + \left(\sum_{f=d,s} P_f(2C_f - 1) - \lambda \sum_{f=u,c} P_f(2C_f - 1) \right)}$$

with the same ratio λ as used in the leptonic analysis. The following result was obtained:

$$A_{FB}^{b\bar{b}} = 0.115 \pm 0.017.$$

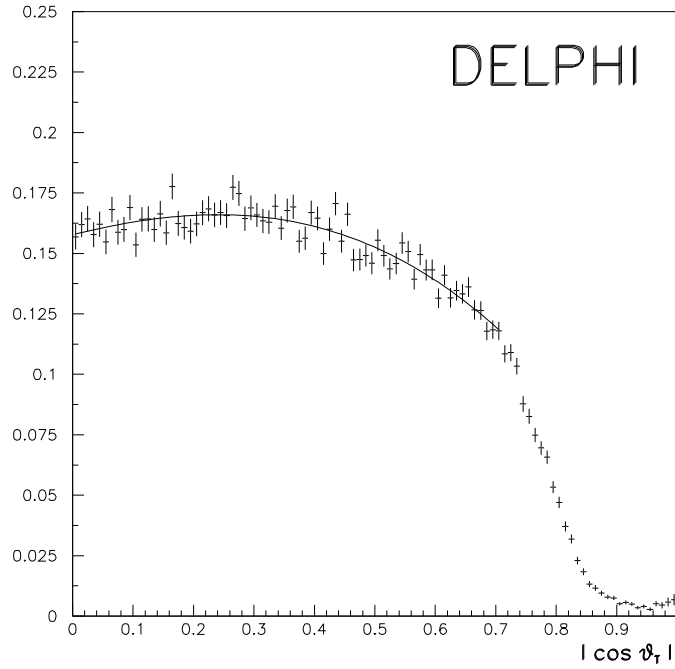


Figure 12: Fraction of selected events as a function of unsigned $\cos\theta_T$.

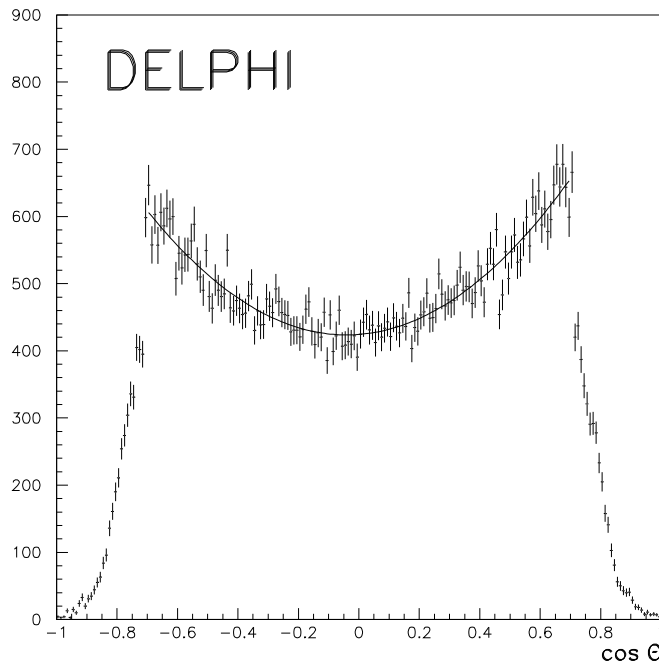


Figure 13: $\cos\Theta$ distribution of the enriched B sample. The result of the fit is also shown. The sign of $\cos\Theta$ is determined from the hemisphere jet charges as described in the text.

4.4 Consistency checks and systematic uncertainties

The possibility of a $\cos\Theta$ dependence of the B -enrichment procedure was studied by repeating the fit in different angular regions. The results are reported in table 11. No significant variations were observed.

The analysis was repeated for different conditions of the tagging probability ($P_H = 0.1, 0.006$), for different momentum powers ($k = 0.2, 1.0$) in the jet charge algorithm, and for two different momentum ranges ($0.5 \text{ GeV}/c < p < 50 \text{ GeV}/c$ and $1 \text{ GeV}/c < p < 50 \text{ GeV}/c$) of charged-particle tracks included in the hemisphere charge evaluation to check its consistency. The analysis was also repeated for a different B -enrichment technique [36] in which at least 3 tracks in one hemisphere were required to have absolute impact parameter larger than $200\mu\text{m}$. This enrichment provided a sample with B -purity of ~ 0.70 . The corresponding results are shown in table 12, where only the statistical errors on $A_{FB}^{b\bar{b}}$ are reported. A larger systematic error is expected for the tagging condition $P_H = 0.10$ because of the lower B enrichment of this sample.

The different systematic uncertainties which affected this measurement could be separated into two categories, one affecting the B -enrichment procedure and the other the hemisphere charge determination. The following effects were considered for the first class:

- the variation of the acceptance correction parameters within their errors;
- the variation of B -enrichment purity within its error.

For the class affecting the probabilities of correct charge assignment C_f , the following sources were considered:

- the statistical and systematic uncertainties in the estimation of C_b discussed in the previous section;
- the possible dependence of C_b on $\cos\theta_T$: the effect was studied allowing different values of C_b for various regions of $\cos\theta_T$ according to the results of figure 10.(b);
- the systematic uncertainties on C_f for u, d, s, c flavours related to the physical parameters of the simulation (charm fragmentation, hadronization ratio $\frac{u}{s}$, Λ_{QCD} , Matrix Element model and the so-called ‘popcorn’ parameter [37]). The variations followed the procedure described in [38].

Finally the systematic uncertainty related to the ratio $\lambda = \frac{A_{FB}^{c\bar{c}}}{A_{FB}^{b\bar{b}}}$ was negligible. The different contributions to the systematic error are listed in table 13. The final result of the analysis with the lifetime tag was:

$$A_{FB}^{b\bar{b}} = 0.115 \pm 0.017(stat.) \pm 0.010(syst.) \pm 0.003(mixing).$$

5 Conclusion

Using Z^0 hadronic decays detected in the DELPHI experiment at LEP, the following results for $A_{FB}^{b\bar{b}}$ have been obtained:

- with the method based on semi-leptonic b decays (1991-1992 data):

$$A_{FB}^{b\bar{b}} = 0.104 \pm 0.013(stat.) \pm 0.004(syst.) \pm 0.003(mixing);$$

- with a lifetime tag method (1992 data):

$$A_{FB}^{b\bar{b}} = 0.115 \pm 0.017(stat.) \pm 0.010(syst.) \pm 0.003(mixing).$$

Angular range	$A_{FB}^{B^-tag}$
$ \cos\Theta \leq 0.70$	0.0302 ± 0.0046
$ \cos\Theta \leq 0.65$	0.0265 ± 0.0050
$ \cos\Theta \leq 0.60$	0.0307 ± 0.0055
$ \cos\Theta \leq 0.50$	0.0292 ± 0.0069
$ \cos\Theta \leq 0.40$	0.0324 ± 0.0093
$0.40 \leq \cos\Theta \leq 0.55$	0.0202 ± 0.0082
$0.55 \leq \cos\Theta \leq 0.70$	0.0342 ± 0.0071

Table 11: Dependence of the asymmetry on different $\cos\Theta$ intervals.

Consistency check	$A_{FB}^{b\bar{b}}$
B enrichment with $F_H < 0.100$	0.095 ± 0.018
B enrichment with $F_H < 0.006$	0.116 ± 0.020
B enrichment of [36]	0.100 ± 0.030
$Q_{Hemisphere}$ with $k=0.2$	0.113 ± 0.021
$Q_{Hemisphere}$ with $k=1.0$	0.123 ± 0.019
$Q_{Hemisphere}$ with $k=0.5, p > 0.5\text{GeV}/c$	0.112 ± 0.018
$Q_{Hemisphere}$ with $k=0.5, p > 1.0\text{GeV}/c$	0.114 ± 0.019

Table 12: Consistency checks on $A_{FB}^{b\bar{b}}$, only the statistical uncertainty is reported. The systematic uncertainties are not obviously the same. In particular for the enrichment cut value $F_H < 0.100$, due to the lower B-purity of the sample, a much bigger systematic uncertainty is expected.

Source of uncertainty	$\Delta A_{FB}^{b\bar{b}}$
Angular acceptance correction	0.002
Purity of the B enrichment	0.005
Statistical uncertainty on C_b	0.007
Systematic uncertainty on C_b	0.002
C_b dependence on $\cos\theta_T$	0.002
Mixing parameter χ	0.003
Fragmentation ($\epsilon_c = 0.064 \pm 0.015$)	0.002
Hadronization ratio $\frac{s}{u}$ (0.27 – 0.36)	0.001
Variation of Λ_{QCD} (240 – 400 MeV)	$< 5 \cdot 10^{-4}$
Matrix Element Monte Carlo	0.001
Variation of the ‘popcorn’ parameter(0.0 – 0.9)	0.001

Table 13: Summary of systematic uncertainties on $A_{FB}^{b\bar{b}}$.

These two results have been combined. An important part ($\sim 65\%$) of the leptonic sample is contained in the lifetime sample but amounts only to 6% of it. This leptonic sample has a different weight in the lifetime analysis due to the different jet-charge characteristics of the B semileptonic decays. However, the relative weight of leptonic to hadronic events in the lifetime analysis has been estimated to be of the order of 10% only. For a statistical correlation below 20%, no observable effect was obtained on the combined result. Therefore the statistical correlation between the two samples was neglected. The combined result is, taking into account the correlation between the systematic uncertainties:

$$A_{\text{FB}}^{\text{b}\bar{\text{b}}} = 0.107 \pm 0.011(\text{stat.} + \text{syst.} + \text{mixing}).$$

A value of $A_{\text{FB}}^{\text{c}\bar{\text{c}}}$ has also been extracted from the lepton sample. Its value is

$$A_{\text{FB}}^{\text{c}\bar{\text{c}}} = 0.083 \pm 0.022(\text{stat.}) \pm 0.016(\text{syst.}).$$

It has a correlation of 0.15 with the combined $A_{\text{FB}}^{\text{b}\bar{\text{b}}}$ value. This value of $A_{\text{FB}}^{\text{c}\bar{\text{c}}}$ is compatible with the $A_{\text{FB}}^{\text{b}\bar{\text{b}}}$ result within the Standard Model framework (as shown in figure 14).

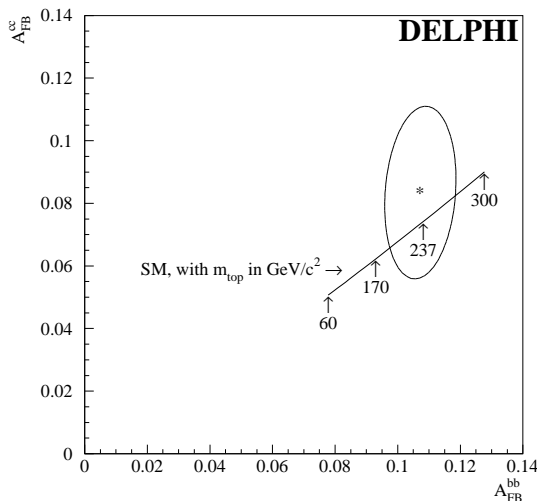


Figure 14: One standard deviation ellipse for the $A_{\text{FB}}^{\text{c}\bar{\text{c}}}$ asymmetry and the combined (lepton + lifetime tag) $A_{\text{FB}}^{\text{b}\bar{\text{b}}}$ asymmetry. The star indicates the central value and the error includes statistical and systematic components. The prediction of the Standard Model with a top mass between 60 GeV/c² and 300 GeV/c² for $m_{\text{Higgs}} = 300 \text{ GeV}/c^2$ is also shown.

A Standard Model fit to the asymmetries obtained in this paper, taking into account their covariance matrix, has been performed using the program ZFITTER [15]. With $M_Z = 91.187 \text{ GeV}/c^2$, $\alpha_s = 0.120$, $m_{\text{Higgs}} = 300_{-240}^{+700} \text{ GeV}/c^2$ and $\sqrt{s} = 91.27 \pm 0.02 \text{ GeV}$, it corresponds to a top-quark mass

$$m_{\text{top}} = 237_{-47}^{+38}(\text{expt.}) \text{ }_{-17}^{+12}(\text{Higgs}) \text{ GeV}/c^2$$

and to an effective weak mixing angle

$$\sin^2 \theta_{\text{eff}}^{\text{lep}} = 0.2294 \pm 0.0021,$$

in agreement with the results of the other LEP experiments [2–5].

Acknowledgements

We are greatly indebted to our technical collaborators and to the funding agencies for their support in building and operating the DELPHI detector, and to the members of the CERN-SL Division for the excellent performance of the LEP collider.

References

- [1] DELPHI collaboration, P. Abreu et al., Phys. Lett. **B276** (1992) 536.
- [2] ALEPH Collaboration, D. Buskulic et al., Z. Phys. **C62** (1994) 179.
- [3] L3 Collaboration, M. Acciarri et al., *Measurement of the $B^0 - \bar{B}^0$ Mixing Parameter and the $Z \rightarrow b\bar{b}$ Forward-Backward Asymmetry*, CERN-PPE/94-89, to be published in Phys. Lett. B.
- [4] OPAL Collaboration, R. Akers et al., Z. Phys. **C60** (1993) 19.
- [5] ALEPH Collaboration, D. Buskulic et al., *A Measurement of $A_{FB}^{b\bar{b}}$ in lifetime tagged Heavy Flavour Z decays*, CERN-PPE/94-84, to be published in Phys. Lett. B.
- [6] A. De Rujula et al., Nucl. Phys. **B138** (1978) 387.
- [7] DELPHI collaboration, P. Abreu et al., Nucl. Instr. Meth. **A303** (1991) 233.
- [8] N. Bingefors et al., Nucl. Instr. Meth. **A328** (1993) 447.
- [9] T. Sjöstrand, Comp. Phys. Comm. **39** (1986) 347;
T. Sjöstrand and M. Bengtsson, Comp. Phys. Comm. **43** (1987) 367;
T. Sjöstrand: JETSET 7.3 manual, preprint CERN-TH6488/92 (1992).
- [10] C. Peterson et al., Phys. Rev. **D27** (1983) 105.
- [11] DELSIM Reference Manual, DELPHI 87-98 PROG 100, Geneva, 1989.
- [12] JADE Collaboration, W. Bartel et al., Z. Phys. **C33** (1986) 23;
JADE Collaboration, S. Bethke et al., Phys. Lett. **B213** (1988) 235.
- [13] DELPHI Collaboration, P. Abreu et al., Z. Phys. **C56** (1992) 47.
- [14] C. Matteuzzi, *Proceedings of the International Europhysics Conference on High Energy Physics*, Marseille, July 1993, Editions Frontieres (1993) 470.
- [15] D. Bardin et al., Z. Phys. **C44** (1989) 493; Nucl. Phys. **B351** (1991) 1;
Phys. Lett. **B229** (1989) 405; Phys. Lett. **B255** (1991) 290;
D. Bardin et al., ZFITTER, an Analytical Program for Fermion Pair Production in e^+e^- Annihilation, CERN-TH 6443/92, May 1992.
- [16] M. Swartz, *High energy tests of the electroweak Standard Model*, To be published in *Proceedings of the XVI International Symposium on Lepton-Photon Interaction*, Cornell, Ithaca, August 1993.
- [17] CLEO Collaboration, S. Henderson et al., Phys. Rev. **D45** (1992) 2212.
- [18] N. Isgur et al., Phys. Rev. **D39** (1989) 799.
- [19] G. Altarelli et al., Nucl. Phys. **B208** (1982) 365.
- [20] W. Venus, *b Weak Interaction Physics in High Energy Experiments*, To be published in *Proceedings of the XVI International Symposium on Lepton-Photon Interaction*, Cornell, Ithaca, August 1993.
- [21] DELPHI Collaboration, P. Abreu et al., *Determination of $\Gamma_{b\bar{b}}$ and $BR(b \rightarrow l)$ using semi-leptonic decays*, Contribution to the *29th rencontres de Moriond*, Meribel, France, March 1994.
- [22] OPAL Collaboration, R. Akers et al., Z. Phys. **C58** (1993) 523.
- [23] ARGUS Collaboration, H. Albrecht et al., Phys. Lett. **B278** (1992) 202.
- [24] DELCO Collaboration, W. Bacino et al., Phys. Rev. Lett. **43** (1979) 1073.
- [25] MARKIII Collaboration, R.M. Baltrusaitis et al., Phys. Rev. Lett. **54** (1985) 1976.
- [26] The LEP Electroweak Working Group, DELPHI 94-23 PHYS 357, Geneva, 1994.
- [27] ALEPH Collaboration, D. Buskulic et al., Z. Phys. **C62** (1994) 1.
- [28] DELPHI Collaboration, P. Abreu et al., Z. Phys. **C59** (1993) 533.
- [29] OPAL Collaboration, R. Akers et al., Z. Phys. **C60** (1993) 601.
- [30] K. Woschnagg, *Asymmetry in production of beauty and charm quark pairs in electron-positron annihilation*, Ph.D. Thesis, Uppsala University (1994).

- [31] DELPHI Collaboration, P. Abreu et al., *Measurement of the $\Gamma_{b\bar{b}}/\Gamma_{had}$ Branching Ratio of the Z by Double hemisphere tagging*, CERN-PPE/94-131, to be published in Z. Phys. C.
- [32] ALEPH Collaboration, D. Buskulic et al., Phys. Lett. **B313** (1993) 535.
- [33] J. Berge et al., Nucl. Phys. **B184** (1981) 13;
JADE Collaboration, T. Greenshaw et al., Z. Phys. **C42** (1989) 1.
- [34] DELPHI Collaboration, P. Abreu et al., Phys Lett. **B322** (1994) 459.
- [35] Review of Particle Properties, Phys. Rev. **D50** (1994) 1173.
- [36] A. Passeri, *Measurement of $A_{FB}^{b\bar{b}}$ using jet charge and lifetime tag*, Ph.D. Thesis, University of Rome (1994).
- [37] A. De Angelis, J. Phys. G: Nucl. Part. Phys. **19** (1993) 1233.
- [38] DELPHI Collaboration, Phys. Lett. **B277** (1992) 371.